

Kernel-based Diffusion Approximated Markov Decision Processes for Off-Road Autonomous Navigation and Control

Junhong Xu¹, Kai Yin², Zheng Chen¹, Jason M. Gregory³, Ethan A. Stump³, Lantao Liu¹

Abstract—We propose a diffusion approximation method to the continuous-state Markov Decision Processes (MDPs) that can be utilized to address autonomous navigation and control in unstructured off-road environments. In contrast to most decision-theoretic planning frameworks that assume fully known state transition models, we design a method that eliminates such a strong assumption that is often extremely difficult to engineer in reality. We first take the second-order Taylor expansion of the value function. The Bellman optimality equation is then approximated by a partial differential equation, which only relies on the first and second moments of the transition model. By combining the kernel representation of the value function, we then design an efficient policy iteration algorithm whose policy evaluation step can be represented as a linear system of equations characterized by a finite set of supporting states. We first validate the proposed method through extensive simulations in 2D obstacle avoidance and 2.5D terrain navigation problems. The results show that the proposed approach leads to a much superior performance over several baselines. We then develop a system that integrates our decision-making framework with onboard perception and conduct real-world experiments in both cluttered indoor and unstructured outdoor environments. The results from the physical systems further demonstrate the applicability of our method in challenging real-world environments.

I. INTRODUCTION

Decision-making of an autonomous mobile robot moving in unstructured environments typically requires the robot to account for uncertain action (motion) outcomes, and at the same time, maximize the long-term return. The Markov Decision Process (MDP) is a very useful framework for formulating such decision-theoretic planning problems [1]. Since the robot is moving in a continuous space, directly employing the standard form of MDP needs a discretized representation of the robot state and action. For example, in practice the discretized robot states are associated with spatial tessellation [2], and a grid-map like representation has been widely used for robot planning problems where each grid is regarded as a discrete state; similarly, actions are simplified as transitions to traversable grids which are usually the very few number of adjacent grids in vicinity.

However, the discretization can be problematic. Specifically, if the discretization is low in resolution (i.e., large but few number of grids), the decision policy becomes a very rough approximation of the simplified (discretized) version



Fig. 1: In unstructured environments, the robot needs to make motion decisions in the navigable space with spatially varying terrestrial characteristics (hills, ridges, valleys, slopes). This is different from the simplified and structured environments where there are only two types of representations, i.e., either obstacle-occupied or obstacle-free. Evenly tessellating the complex terrain to create a discretized state space cannot effectively characterize the underlying value function used for computing the MDP solution. (Picture credit: NASA)

of the original problem; on the other hand, if the discretization is high in resolution, the result might be approximated well, but this will induce prohibitive computational cost and prevent the real-time decision-making. Finally, the characteristics of state space might be complex and it is inappropriate to conduct lattice-like tessellation which is likely to result in sub-optimal solutions. See Fig. 1 for an illustration.

Another critical issue lies in MDP's transition model, which describes the probabilistic transitions from a state to others. However, obtaining an accurate probability distribution function for robot motion transitions is oftentimes unrealistic even without considering spatiotemporal variability. This is another important factor that significantly limits the applicability of MDP in many real-world problems. Reinforcement learning [3] does not rely on a transition model specification, but requires a large number of training trials to learn the value function and the policy, which can be viewed as another strong and difficult assumption in many robotic missions. Thus, it is desirable that the demanding assumption of the known transition probability function can be relaxed as some non-exact form and can be obtained without cumbersome learning trials. This can be achieved by leveraging the major characteristics of the transition probabilistic distribution (e.g., moments or quantile of the distribution), which typically can be obtained (well

¹Luddy School of Informatics, Computing, and Engineering at Indiana University, Bloomington, IN 47408, USA. E-mail: {xu14, zc11, lantao}@iu.edu.

²Expedia Group. E-mail: kyin@expediagroup.com.

³Army Research Laboratory. E-mail: {jason.m.gregory1, ethan.a.stump2}.civ@cvr.mil.

approximated) from lightweight historical data or offline tests [2]. If we only assume such “partial knowledge” – first two moments – of the transition model, we must re-design the modeling and solving mechanisms.

To address the above problems, we propose a diffusion-approximated and kernel-based solution. Our primary focus is to develop a theoretically-sound and practically-efficient solution to compute the optimal value function in continuous-state MDPs without requiring a full probabilistic transition model.

Our contributions can be summarized as follows:

- First, to relax the requirement of fully known transition functions, we apply the second-order Taylor expansion to the value function. The Bellman-type policy evaluation equation and Bellman optimality equation are then approximated by a diffusion-type partial differential equation (PDE) which only relies on the first and second moments of transition probability distribution. The solution of the Taylored Bellman optimality equation can be viewed as a infinite-horizon discounted reward diffusion process.
- Second, to improve both the efficiency and the flexibility of the value function approximation, we use kernel functions which can represent a large number of function families for better value approximation. This approximation can conveniently characterize the underlying value functions with a finite set of discrete supporting states, leading to fast computation.
- Finally, we develop an efficient policy iteration algorithm by integrating the kernel value function representation and the Taylor-based diffusion-type approximation to Bellman optimality equation. The policy evaluation step can be represented as a linear system of equations with characterizing values at the finite supporting states, and the only information needed is the first and second moments of the transition function. This alleviates the need for heavily searching in continuous/large state space and the need for carefully modeling/engineering the transition probability.

The organization of the paper is as follows: we review the relevant literature and provide background in formulating stochastic planning problems and value function approximation methods in Section II and III, respectively. In Section IV, we present the Taylored Bellman equation and the proposed policy iteration algorithm. Section V provides evaluation results for various important algorithmic properties of the proposed method. Then, we integrate the perception into our framework to build an autonomy system and demonstrate real-world experiments in Section VI–VIII. Finally, we conclude the paper and discuss insights learned from the real-world experiments in Section IX.

II. RELATED WORK

In this section, we first provide a brief survey on the value function approximation in Markov Decision Processes (MDPs). Then, we review deterministic and stochastic path

and motion planning methods developed in the robotics community. We highlight our contributions at last.

A. Value Function Approximation in Continuous-State MDPs

Motion planning under action uncertainty can be formulated as an MDP with continuous state and action [4], [5]. Many existing works focus on value function representation and approximation in large/continuous state space [3], [5]. Unlike in the discrete state space, the value function in the continuous (or large) state space requires an infinite-sized table. Additionally, computing state-values requires enumeration over every entry, which is practically impossible [5]. In general, approximation of the value function is needed to avoid this intractability when storing and computing the value function over the continuous state space.

One simple approach to approximating the value function is by tessellating the continuous state space into uniform grids. This method is popular in many robotic applications [6], [7], [8], [9], [10]. However, this uniform tessellation approach does not scale well to environments with complex geometric structures, and it requires a large number of grids when the problem size increases, known as the curse of dimensionality [11]. A more advanced discretization technique that alleviates this problem is by adaptive discretization [12], [13], [14], [15], [16].

Alternative methods tackle this challenge through representing and also approximating the value function by a linear combination of basis functions or some parametric functions [17], [5], [18]. The weights in the linear combination can be optimized by minimizing the Bellman residual [19]. However, these methods are not applicable in complicated problems because selecting a proper set of basis functions is non-trivial. This weakness may be resolved through kernel methods [20]. Because the weights in linear combination of basis functions can be presented by their product (through so-called dual form of least squares [21]), the product may be better replaced by kernel functions (on so-called reproducing kernel Hilbert spaces) at supporting states. Once value functions at supporting states are obtained, the approximation to value function at any state is also determined. In [22], the authors use a Gaussian process with a Radial Basis Kernel (RBF) to approximate the value function. This approach to approximating the value function by kernel functions is referred as the *direct kernel-based method* in this paper. There is a vast literature on kernelized value function approximations in reinforcement learning [23], [24], [25], [26]. But few studies in robotic planning problems leveraged this approach. A recent application of work [23] on marine robots can be found in [27]. In addition, due to the advancement in deep learning, using neural networks to approximate value function has demonstrated successes in a wide range of applications [28]. However, it is generally hard to find suitable network architectures and hyperparameters to approximate the value function [29] for different environments and robotic motion planning tasks.

Unfortunately, all these approaches rely on either fully known transitions in MDP or the selection of basis functions, which are difficult to obtain in practice. Therefore, the challenge becomes *how to design a principled methodology without explicitly relying on basis functions and without full knowledge of transitions in MDP, which will be addressed in this work.*

B. Deterministic and Stochastic Planning in Robotics

Most of the traditional robotic planning methods (see [30] for a recent survey) use a simplified deterministic robot motion model, e.g., holonomic kinematics, to compute an open-loop path, e.g., sampling-based motion planners such as probabilistic roadmap (PRM) and rapidly exploring random tree (RRT) and their variants [16], [31]. Since the modeling error exists between the model used in planning and the real world, the robot cannot execute the path directly and requires a separate controller to track the path. To ensure the path is trackable by the controller, refining the planned path into a kinodynamically trackable trajectory [32] is necessary. One strategy to generate such trajectories is based on trajectory optimization. Existing trajectory optimization methods can be categorized into hard-constrained methods and soft-constrained methods. Using hard-constrained optimization technique to solve trajectory generation problem has been proposed by [33], where piecewise polynomial trajectories are generated by solving a quadratic programming (QP) problem. A closed-form solution is provided to solve an unconstrained QP problem, and intermediate waypoints are added iteratively to ensure the safety of the trajectories [34]. Free space represented by multiple geometric volumes, e.g., cubes [35], [36], spheres [37], [38], and polyhedra [39], [40], are used to formulate a convex optimization problem, which generates smooth trajectories within the volumes. However, hard-constrained methods ignore the distance information to the obstacle boundaries and are prone to generate trajectories close to the obstacles. Such safety issue motivates the development of the soft-constrained methods which leverage the distance gradient during optimization such that the trajectories could be adjusted to stay far from obstacle boundaries while maintaining the smoothness property [41], [42], [43].

The above design of the navigation system is based on deterministic models at all levels, i.e., from path planning to trajectory optimization, and uncertainties in the motion are entirely handled by the tracking controller. Such decoupled design is brittle because it is possible that the feedback controller cannot stabilize the open-loop path computed by the planner. Therefore, to reduce the burden of designing and tuning separate controllers for different environments, it is desirable to develop methods that directly consider the action execution uncertainty during the planning phase if the error between the planning model and the real-world action is large. This problem is particularly obvious when the robot moves on rough terrains.

Early work of stochastic planning in the robotics community was mostly built upon the sampling-based motion planning paradigm. In [44], the authors compute local feed-

back controllers while adding new tree branches in the RRT algorithm to stabilize the robot's motion between two tree nodes. A similar idea has also been exploited by [45] with a different planner and controller. This method considers both the sensing and motion uncertainty and uses the linear-quadratic Gaussian (LQG) controller [46] to stabilize the motion and sensing uncertainties along the edges generated by a PRM algorithm. Alternatively, [47] use the LQG controller to compute a distribution of paths, from which the path is planned by the RRT algorithm that optimizes an objective function based on the path distribution. Instead of modular design of the planning and control components, [48] propose a more integrated approach to solving the general continuous-time stochastic optimal control problem. The method first approximates the original MDP by a discrete MDP through sampling points in the state space, and then a closed-loop policy is computed in this discrete MDP. The approximation and solution are then refined by iterating this sampling and solving procedure.

Model predictive control (MPC), or receding horizon control, is another strategy to resolve motion uncertainty [49], [50]. At each timestep, it solves a finite horizon optimal control problem and applies the first action of the computed open-loop trajectory online. To reduce computational burden, MPC usually uses a deterministic model to predict future states [51]. Robust MPC [52] explicitly deals with the model uncertainty by optimizing over feedback policies rather than open-loop trajectories. However, this optimization is computationally expensive. Thus, in practice, tube MPC that focuses only on a sub-space is often used as an approximate solution to robust MPC [53]. Tube MPC for nonlinear robot motion models is still an active research area. For example, sum-of-squared programming [54], [55] and reachability analysis [56], [57] are used for solving the nonlinear Tube MPC problem. More recently, Model Predictive Path Integral (MPPI) control [58], [59], [60], [59], [61], a sampling-based MPC approach to solve finite-horizon stochastic optimal control problems with arbitrary cost function and nonlinear system dynamics is developed.

In general, robot motion planning essentially requires to reason about uncertainties during motion control. However, because the prohibitive computation prevents the robot from real-time decision, most of the traditional approaches to generating feasible trajectories do not consider uncertainties. Oftentimes some heuristics are leveraged to ensure the motion safety during execution, e.g., using the soft-constrained methods. In contrast, our proposed framework solves the stochastic planning problem in a direct and integrative fashion. As a result, the computed policy can naturally guide the robot with a large clearance from the obstacles, without adding extra penalty in the objective function which can be hard to specify in practice. In addition, most existing methods that solve the stochastic planning problems avoid the difficulties in directly computing the optimal value function through using arbitrary, e.g., non-linear or discontinuous, reward and transition functions. Different from that, the proposed approach makes the direct computation possible in

practice, which opens a new line of work to solve stochastic motion planning problems.

III. PRELIMINARY BACKGROUND

A. Markov Decision Processes

We formulate the robot decision-theoretic planning problem as an infinite horizon discrete time discounted Markov Decision Process (MDP) with continuous states and finite actions. It is defined by a 5-tuple $\mathcal{M} \triangleq \langle \mathbb{S}, \mathbb{A}, T, R, \gamma \rangle$, where $\mathbb{S} = \{s\} \subseteq \mathbb{R}^d$ is the d -dimensional continuous state space and $\mathbb{A} = \{a\}$ is a finite set of actions. \mathbb{S} can be thought of as the robot workspace in our study. A robot transits from a state s to the next s' by taking an action a in a stochastic environment and obtains a reward $R(s, a)$. Such transition is governed by a conditional probability distribution $T(s, a, s') \triangleq p(s'|s, a)$ which is termed as transition model (or transition function); the reward $R(s, a)$, a mapping from a pair of state and action to a scalar value, which specifies the one-step objective that the robot receives by taking action a at state s . The final element $\gamma \in (0, 1)$ in \mathcal{M} is a discount factor which will be used in the expression of value function.

We consider the class of deterministic policies Π , which defines a mapping $\pi \in \Pi : \mathbb{S} \rightarrow \mathbb{A}$ from a state to an action. The expected discounted cumulative reward for any policy π starting at any state s is expressed as

$$v^\pi(s) = \mathbb{E} \left[\sum_{t=0}^{\infty} \gamma^t R(s_t, \pi(s_t)) | s_0 = s \right]. \quad (1)$$

The state at the next time step, s_{t+1} , draws from distribution $p(s_{t+1}|s_t, \pi(s_t))$. Let us use k to denote the computation epoch, then we can rewrite the above equation recursively as follows

$$v_{k+1}^\pi(s) = R(s, \pi(s)) + \gamma \mathbb{E}^\pi[v_k^\pi(s')|s] \triangleq \mathcal{B}^\pi v_k^\pi(s), \quad (2)$$

where \mathcal{B}^π is called the *Bellman operator*, and $\mathbb{E}^\pi[v_k^\pi(s')|s] = \int p(s'|s, \pi(s)) v_k^\pi(s') ds'$. The computation epoch k is omitted in the rest of the paper for notation simplicity. Eq. (2) is called Bellman equation. The function $v^\pi(s)$ is usually called the *state value function* of the policy π . Solving an MDP amounts to finding the optimal policy π^* with the optimal value function which satisfies the *Bellman optimality equation*

$$v^{\pi^*}(s) = \max_{\pi} \{R(s, \pi(s)) + \gamma \mathbb{E}^\pi[v^\pi(s')|s]\}. \quad (3)$$

B. Approximate Policy Iteration via Value Function Representation

Value iteration and policy iteration are the most prevalent approaches to solving an MDP. It has been shown that the value iteration and policy iteration can both converge to the optimal policy in MDPs with discrete states [4], [5]. Our work will be built upon policy iteration and here we provide a summary of the common value function approximation methods used in policy iteration when dealing with continuous states [62], [63], [64].

Policy iteration requires an initialization of the policy (can be random). When the number of states in the MDP is finite, a system of finite number of linear equations can be established based on the initial policy, where each equation is exactly the value function (Eq. (2)). The solution to this linear system yields state-values for all states of the initial policy [65]. This step is called *policy evaluation*. The second step is to improve the current policy by greedily improving local actions based on the incumbent values obtained. This step is called *policy improvement*. Through iterating these two steps, we can find the optimal policy and a unique solution to the value function that satisfies Eq. (1) for every state.

If, however, the states are continuous or the number of states is infinite, it is intractable to store and evaluate the value function at every state. One must resort to approximate solutions by finding an appropriate representation of the value function. Suppose that the value function can be represented by a weighted linear combination of known functions where only weights are to be determined, then a natural way to go is leveraging the Bellman-type equation, i.e., Eq. (2), to compute the weights. Specifically, given an arbitrary policy, the representation of value function can be evaluated at a finite number of states, leading to a linear system of equations whose solutions can be viewed as weights [66]. This obtained representation of value function can be used to improve the current policy. The remaining procedure is then similar to the standard policy iteration method. The final obtained value function representation serves as an approximated optimal value function *for the whole continuous state space*, and the corresponding policy can be obtained accordingly.

Formally, let the value function approximation under policy π be

$$v^\pi(s) \simeq v(s; w^\pi) = \sum_{i=1}^m w_i^\pi \cdot \phi_i(s), \quad (4)$$

where $\phi_i \in \Phi \triangleq \{\phi_1, \dots, \phi_m\}$. The elements in the set Φ are called the *basis functions* in literature [62], and these basis functions are usually parametric functions with a fixed form. A finite number of supporting states $\mathbf{s} = \{s^1, \dots, s^N\}$, $N > m$ can be selected. The selection of supporting states \mathbf{s} needs to take into account the characteristics of the underlying value functions. In the scenario of robot motion planning in complex terrains, it relates to the properties of the terrain, e.g., geometry or texture. The solution to w^π can be calculated by minimizing the squared *Bellman error* over \mathbf{s} , defined by $\mathcal{L}(w^\pi) = \sum_{i=1}^N (v(s^i; w^\pi) - \mathcal{B}^\pi v(s^i; w^\pi))^2$. And w^π may have a closed form solution in terms of the basis functions, transition probabilities, and rewards [66]. By policy iteration, the final solution for $v(s; w^\pi)$ can be obtained. Note that $v(s)$ may also be approximated by any non-parametric nonlinear functions such as neural networks.

IV. METHODOLOGY

Our objective is to design a principled kernel-based policy iteration approach by leveraging kernel methods to solve

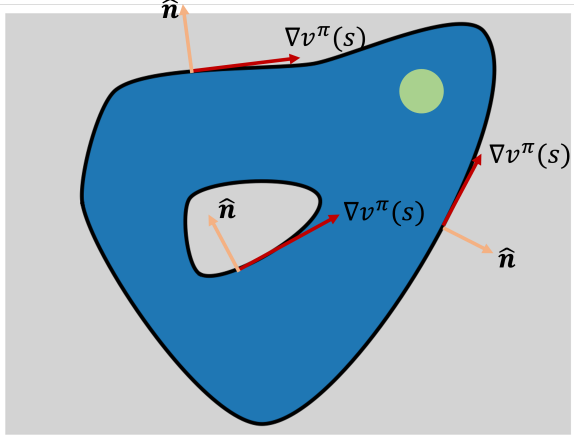


Fig. 2: Illustration of the boundary condition in Eq. (8a) using a 2D example. The blue and green regions indicate the state space and the goal region, respectively. The grey areas represent the infeasible space, e.g., obstacles, and the boundaries are shown as black curves. The normal vector \hat{n} and the gradient of value function $\nabla v^\pi(s)$ at three arbitrary boundary points are indicated by yellow and red arrows, respectively.

the continuous-state MDP. In contrast to most decision-theoretic planning frameworks which assume fully known MDP transition probabilities [1], [65], we propose a method that eliminates such a strong premise which oftentimes is extremely difficult to engineer in practice. To overcome this challenge, first we apply the second-order Taylor expansion of the kernelized value function (Section IV-A). The Bellman optimality equation is then approximated by a partial differential equation which only relies on the first and second moments of transition probabilities (Section IV-B). Combining the kernel representation of value function, this approach efficiently tackles the continuous or large-scale state space search with minimum prerequisite knowledge of state transition model (Sections IV-C and IV-D).

A. Tailored Approximate Bellman Equation

To design an efficient approach for solving continuous-state MDP problems, we essentially need to fulfill two requirements: *a suitable representation of the value function* and *efficient computation of the Bellman optimality equation*.

For the first requirement, we may directly apply the basis functions to approximate the value function and then solve the Bellman optimality equation. Yet this approach faces difficulties of explicitly specifying basis functions. If the set of basis functions is not rich enough, the approximation error can be large. A better approach may be a direct application of kernel methods to represent the value function (referred as the *direct kernel-based method*). We will discuss this method later. But this representation does not satisfy the second requirement, i.e., efficient evaluation of the Bellman optimality equation. This is because a fully specified transition probability function $p(\cdot|\cdot, \cdot)$ is required for computing the Bellman

operator, but it is usually hard to specify in the real world. In addition, even this transition function can be obtained, the expectation $\mathbb{E}^\pi[v_k^\pi(s')] = \int p(s'|s, \pi(s))v_k^\pi(s')ds'$ generally does not have a closed-form solution, and computationally expensive numerical integration is typically entailed.

In contrast to directly solving Eq. (3) by value function approximation, we consider an approximation to the Bellman-type equation at first and then apply value function approximation. We approximate the Bellman equation by using only first and second moments of transition functions. This will allow us to obtain a nice property that a complete and accurate transition model is not necessary; instead, only the important statistics such as mean and variance (or covariance) will be sufficient for most real-world applications. Additionally, we will see that evaluating the integration over the global state space is not needed. From this perspective, our approximation can be viewed as a local version of the original Bellman equation, i.e., it uses local gradient information to approximate the integral of the value function over possible next states.

Formally, we assume that the state space is of d -dimension and a state s may be expressed as $s = [s_1, s_2, \dots, s_d]^T$. Suppose that the value function $v^\pi(s)$ for any given policy π has continuous first and second order derivatives (this can usually be satisfied with aforementioned value function designs). We subtract both hand-sides by $v^\pi(s)$ from Eq. (2) and then take Taylor expansions of value function around s up to second order [67]:

$$\begin{aligned} & -R(s, \pi(s)) \\ &= \gamma (\mathbb{E}^\pi[v^\pi(s') | s] - v^\pi(s)) - (1 - \gamma) v^\pi(s) \\ &= \gamma \int p(s'|s, \pi(s))(v^\pi(s') - v^\pi(s)) ds' - (1 - \gamma) v^\pi(s) \\ &\simeq \gamma \left((\mu_s^\pi)^T \nabla v^\pi(s) + \frac{1}{2} \nabla \cdot \sigma_s^\pi \nabla v^\pi(s) \right) - (1 - \gamma) v^\pi(s), \end{aligned} \quad (5)$$

where μ_s^π and σ_s^π are the first moment (i.e., a d -dimensional vector) and the second moment (i.e., a d -by- d matrix) of transition functions, respectively, with the following form

$$(\mu_s^\pi)_i = \int p(s'|s, \pi(s))(s'_i - s_i) ds', \quad (6a)$$

$$(\sigma_s^\pi)_{i,j} = \int p(s'|s, \pi(s))(s'_i - s_i)(s'_j - s_j) ds', \quad (6b)$$

for $i, j \in \{1, \dots, d\}$; the operator $\nabla \triangleq [\partial/\partial s_1, \dots, \partial/\partial s_d]^T$ and the notation \cdot in the last equation indicate an inner product; the operator $\nabla \cdot \sigma_s^\pi \nabla$ is read as

$$\nabla \cdot \sigma_s^\pi \nabla = \sum_{i,j} \sigma_{s_i s_j}^\pi \frac{\partial^2}{\partial s_i \partial s_j}.$$

To be concrete, we take a surface-like terrain for example and use that surface as the decision-theoretic planning workspace, i.e., $s = [x, y]^T \triangleq [s_x, s_y]^T$. We have the

expression for the following operator

$$\nabla \cdot \sigma_s^\pi \nabla = \sigma_{xx}^\pi \frac{\partial^2}{\partial x^2} + \sigma_{xy}^\pi \frac{\partial^2}{\partial x \partial y} + \sigma_{yx}^\pi \frac{\partial^2}{\partial y \partial x} + \sigma_{yy}^\pi \frac{\partial^2}{\partial y^2}.$$

Since Eq. (5) approximates calculation of Eq. (2) in the policy evaluation stage, the solution to Eq. (5) thus provides the value function approximation under current policy π . Eq. (5) also implies that we only need to use the first $(\mu_s^\pi)_i$ and second $(\sigma_s^\pi)_{i,j}$ moments instead of computing the expectation of the value function using the original transition model $p(s'|s, \pi(s))$ to evaluate the Bellman operator Eq. (3) required in solving MDPs.

B. Approximate Bellman Optimality Equation via Diffusion-type PDE

Eq. (5) is a diffusion-type partial differential equation (PDE). It is an approximation to the Bellman equation (7) through the second-order Taylor expansion. We will need to solve this PDE to obtain an approximation methodology to the Bellman optimality equation. Typically if solutions exit for a PDE, there could be infinite solutions to satisfy the the PDE unless we impose proper boundary conditions [68]. Therefore, we need to analyze the necessary boundary conditions to Eq. (5).

In our problem settings, robots are not allowed to move out of free-space boundaries. We first observe that the value function should not have values outside of the feasible planning region, i.e., the state space \mathbb{S} , and the value function should not increase towards the boundary of the region. Otherwise it will result in actions that guide the robot outside the free space. A practical boundary condition to impose can be that the directional derivative of the value function with respect to the outward unit normal at the boundary states is zero (see Fig. 2 for an illustration). It is not the only condition that we can impose, but it is a relatively easier condition to obtain solutions with desired behaviors. Second, in order to ensure that the robot is able to reach the goal, we follow the conventional goal-oriented decision-theoretical planning setup and constrain the value function at the goal state to the maximum state-value in the state space \mathbb{S} . These boundary conditions ensure that the policy does not control the robot outside of the feasible regions (safety) and also leads the robot to the goal area.

Formally, let us denote the boundary of entire continuous planning region by $\partial\mathbb{S}$ and the goal state by s_g . Suppose the value function at s_g is v_g . Section IV-A implies that the Bellman optimality equation Eq. (3) can be approximated by the following PDE:

$$0 = \max_{\pi} \left\{ \gamma \left((\mu_s^\pi)^T \nabla v^\pi(s) + \frac{1}{2} \nabla \cdot \sigma_s^\pi \nabla v^\pi(s) \right) + R(s, \pi(s)) - (1 - \gamma) v^\pi(s) \right\}, \quad (7)$$

with boundary conditions

$$\sigma_s^\pi \nabla v^\pi(s) \cdot \hat{\mathbf{n}} = 0, \text{ on } \partial\mathbb{S} \quad (8a)$$

$$v^\pi(s_g) = v_g, \quad (8b)$$

where $\hat{\mathbf{n}}$ denotes the unit vector normal to $\partial\mathbb{S}$ pointing outward, and condition (8a) constrains the directional derivative with respect to this normal vector $\hat{\mathbf{n}}$ to be zero. The solution v^π of the above PDE can be interpreted as a diffusion process with μ_s^π and σ_s^π as drift and diffusion coefficients, respectively. We show a 2D example of this boundary condition in Fig. 2. The normal vectors $\hat{\mathbf{n}}$ at the boundary are perpendicular to the gradient of the value function $\nabla v^\pi(s)$, which constrains the value function from expanding outside the boundaries of the state space. In addition, the direction of each gradient vector points toward the goal, and this allows the policy to follow the value function gradient which guides the robot to move in the goal direction.

The condition (8a) is a type of homogeneous Neumann condition, and condition (8b) can be thought of as a Dirichlet condition in literature [68]. This elegantly approximates the classic Bellman optimality equation by a convenient PDE representation. While Eq. (7) is a nonlinear PDE (due to the maximum operator over all policies), our algorithm in the future section will allow to solve a linear PDE for a fixed policy. In the next section, we will leverage the kernelized representation of the value function to avoid difficulties of directly solving PDE. The kernel method will help transform the problem to a linear system of equations with unknown values at the finite supporting states.

C. Kernel Taylor-Based Approximate Policy Evaluation

With aforementioned formulations, another critical research question is whether the value function can be represented by some special functions that are able to approximate large function families in a convenient way. We tackle this question by using a kernel method to represent the value function. Thanks to Eq. (7) which allows us to extend with kernelized policy evaluation for Taylored value function approximation.

Specifically, let $k(\cdot, \cdot)$ be a generic kernel function[†] [20]. For a set of selected finite supporting states $\mathbf{s} = \{s^1, \dots, s^N\}$, let \mathbf{K} be the Gram matrix with $[\mathbf{K}]_{i,j} = k(s^i, s^j)$, and $\mathbf{k}(\cdot, \mathbf{s}) = [k(\cdot, s^1), \dots, k(\cdot, s^N)]^T$. Given a policy π , assume the value functions at \mathbf{s} are $V^\pi = [v^\pi(s^1), \dots, v^\pi(s^N)]^T$. Then, for any state s' , the kernelized value function has the following form

$$v^\pi(s') = \mathbf{k}(s', \mathbf{s})^T (\lambda \mathbf{I} + \mathbf{K})^{-1} V^\pi, \quad (9)$$

where $\lambda \geq 0$ is a *regularization factor*. When $\lambda = 0$, it links to the kernel ordinary least squares estimation of w^π in Eq. (4); when $\lambda > 0$, it refers to the ridge-type regularized kernel least squares estimation [21]. Furthermore, Eq. (9) implies that as long as the values V^π are available, the value function for any state can be immediately obtained. Now our objective is to get V^π through Eq. (5) and boundary conditions Eq. (8).

[†] It is worth mentioning that our approach of utilizing kernel methods is to approximate the function. This usage should be distinguished from that in the machine learning literature where kernel methods are used to learn patterns from data.

Plugging the kernelized value function representation into Eq. (5), we end up with the following linear system:

$$\left(\mathbf{M}^\pi (\lambda \mathbf{I} + \mathbf{K})^{-1} - (1 - \gamma) \mathbf{I}\right) \mathbf{V}^\pi = \mathbf{R}^\pi, \quad (10)$$

where \mathbf{I} is an identity matrix, \mathbf{R}^π is a $N \times 1$ vector with element $[\mathbf{R}^\pi]_i = -R(s^i, \pi(s^i))$, and \mathbf{M}^π is a matrix whose elements are:

$$[\mathbf{M}^\pi]_{i,j} = \gamma \left((\mu_{s^i}^\pi)^T \nabla_{s^i} + \frac{1}{2} \nabla_{s^i} \cdot \sigma_{s^i}^\pi \nabla_{s^i} \right) k(s^i, s^j). \quad (11)$$

Note that ∇_{s^i} indicates the derivatives with respect to s^i , i.e., $\nabla_{s^i} \triangleq [\partial/\partial s_1^i, \dots, \partial/\partial s_d^i]^T$. Here, we provide a concrete derivation of using the Gaussian kernel to our proposed kernel Taylor-Based approximate method as it is a commonly used kernel in practice and often used in the studies of kernel methods.

Gaussian kernel functions on states s' and s have the form $k(s', s) = c \times \exp\left((- \frac{1}{2}(s' - s)^T \Sigma_s^{-1}(s' - s)\right)$, where c is a constant and Σ_s is a covariance matrix. Note that Σ_s is referred to as the length-scale parameter in our work. The lengthscale governs the “smoothness” of the function, and a large lengthscale leads to a smooth function whereas a small lengthscale causes a rugged function. Due to limited space, we only provide formula below for the first and second derivatives of the Gaussian kernel functions. These formula are necessary when Gaussian kernels are employed (for example, Eq.(11)). In fact, we have

$$\nabla_{s'} k(s', s) = -\Sigma_s^{-1}(s' - s)k(s', s), \quad (12)$$

and

$$\begin{aligned} \nabla_{s'} \cdot \sigma_s \nabla_{s'} k(s', s) &= -\text{tr}(\sigma_s \Sigma_s^{-1}) k(s', s) \\ &+ (s' - s)^T \Sigma_s^{-T} \sigma_s \Sigma_s^{-1}(s' - s) k(s', s), \end{aligned} \quad (13)$$

where $\text{tr}(\cdot)$ denotes the trace of the matrix. By plugging Eq. (12) and Eq. (13) into Eq. (11), we can obtain a closed-form expression for the elements in the matrix \mathbf{M}^π .

The solutions to the system Eq. (10) yield values of \mathbf{V}^π . These values further allow us to obtain the value function (9) for any state under current policy π . This completes modeling our kernel Taylor-based approximate policy evaluation framework.

D. Kernel Taylor-Based Approximate Policy Iteration

With the above formulations, our next step is to design an implementable algorithm that can solve the continuous-state MDP efficiently. We extend the classic policy iteration mechanism which iterates between the policy evaluation step and the policy improvement step until convergence to find the optimal policy as well as its corresponding optimal value function.

Because our kernelized value function representation depends on the finite number of supporting states \mathbf{s} instead of the whole state space, we only need to improve the policy on \mathbf{s} . Therefore, the policy improvement step in the $(k+1)$ -th iteration is to improve the current policy at each support

Algorithm 1 Kernel Taylor-Based Approximate Policy Iteration

Input: A set of supporting states $\mathbf{s} = \{s^1, \dots, s^N\}$; the kernel function $k(\cdot, \cdot)$; the regularization factor λ ; the MDP $\langle \mathbb{S}, \mathbb{A}, T, R, \gamma \rangle$.

Output: The kernelized value function Eq. (9) for every state and corresponding policy.

- 1: Initialize the action at the supporting states.
 - 2: Compute the matrix $\mathbf{K} + \lambda \mathbf{I}$ and its inverse.
 - 3: **repeat**
 - 4: // Policy evaluation step
 - 5: Solve for \mathbf{V}^π according to Eq. (10) in Section IV-A.
 - 6: // Policy improvement step
 - 7: **for** $i = 1, \dots, N$ **do**
 - 8: Update the action at the supporting state s^i based on Eq. (14).
 - 9: **end for**
 - 10: **until** actions at the supporting states do not change.
-

state

$$\begin{aligned} \pi_{k+1}(s) &= \arg \max_{a \in \mathbb{A}} \left\{ R(s, a) + \right. \\ &\quad \left. \gamma \left((\mu_s^a)^T \nabla + \frac{1}{2} \nabla \cdot \sigma_s^a \nabla \right) v^{\pi_k}(s) \right\}, \end{aligned} \quad (14)$$

where $s \in \mathbf{s}$, π_k and π_{k+1} are the current policy and the updated policy, respectively. Note that μ_s^a and σ_s^a depend on a through the transition function $p(s'|s, a)$ in Eq. (6). Compared with the approximated Bellman optimality equation (Eq. (7)), Eq. (14) drops the term $(1 - \gamma)v^{\pi_k}(s)$. This is because $v^{\pi_k}(s)$ does not explicitly depend on action a . The value function of the updated policy satisfies $v^{\pi_{k+1}}(s) \geq v^{\pi_k}(s)$ [4]. If the equality holds, the iteration converges.

The final kernel Taylor-based policy iteration algorithm is pseudo-coded in Alg. 1. It first initializes the actions at the finite supporting states and then iterates between policy evaluation and policy improvement. Since the supporting states as well as the kernel parameters do not change, the regularized kernel matrix and its inverse are computed only once at the beginning of the algorithm. This greatly reduces the computational burden caused by matrix inversion. Furthermore, due to the finiteness of the supporting states, the entire algorithm views the policy π as a table and only updates the actions at the supporting states using Eq. (14). The algorithm stops and returns the supporting state values when the actions are stabilized. We can then use these state-values to get the final kernel value function that approximates the optimal solution. The corresponding policy for every continuous state can then be easily obtained from this kernel value function [69].

Intuitively, this proposed framework is efficient and powerful due to the following reasons: (1) by approximating the Bellman-type equation using the PDE, we eliminate the necessity in requiring a full transition function and the difficulty in computing the expectation over the next state-values; (2) rather than tackling the difficulties in solving

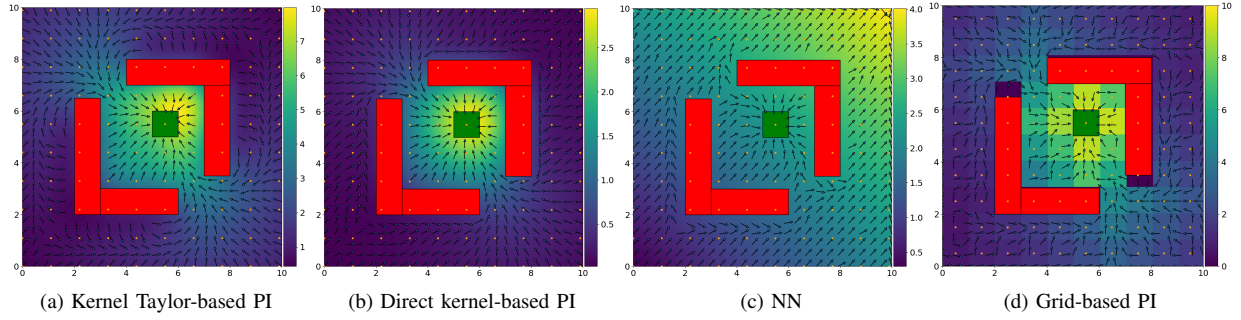


Fig. 3: Evaluation with a traditional simplified scenario where obstacles and goal are depicted as red and green blocks, respectively. We compare the final value function and the final policy obtained from (a) kernel Taylor-based PI, (b) direct kernel-based PI, (c) NN, and (d) grid-based PI. A brighter background color represents a higher state value. The policies are the arrows (vector fields), and each arrow points to some next waypoint. Orange dots denote supporting states or the grid centers (in the case of grid-based PI).

the PDE, we use the kernel representation to convert the problem to a system of linear equations with characterizing values at the finite discrete supporting states. From this viewpoint, our proposed method nicely balances the trade-off between searching in finite states and that in infinite states. In other words, our approach leverages the kernel methods and Bellman optimal conditions under practical assumptions.

V. ALGORITHMIC PERFORMANCE EVALUATION

Before testing the applicability of our proposed method in real-world environments, we conducted algorithmic evaluations in two sets of simulations in order to validate the efficiency of the proposed framework.

To do so, we eliminate the real-world complexities that are not the focus of the main method (e.g., perception, partial observability, and online re-planning). The first evaluation (Section V-A) is a goal-oriented planning problem in a simple environment with obstacle-occupied and obstacle-free spaces. In the second evaluation (Section V-B), we demonstrate that our method can be applied to a more challenging navigation scenario on Mars surface [70], where the robot needs to take into account the elevation of the terrain surface (i.e., “obstacles” become continuous and are implicit).

A. Plane Navigation

1) *Setup*:: Our first test is a 2D plane navigation problem, where the obstacles and the goal area are represented in a $10m \times 10m$ environment, as shown in Fig. 3. The state space for this task is a 2-dimensional Euclidean space, i.e., $s = [s_x, s_y]^T$ and $s \in \mathbb{S} \subseteq \mathbb{R}^2$. The action space is a finite set with a number of Q points $\mathbb{A}(s) = \{a_i(s) | i \in \{1, \dots, Q\}\}$. Each point $a_i(s) = [s_x + r \cos(\frac{2\pi i}{Q}), s_y + r \sin(\frac{2\pi i}{Q})]^T$ is an action generated on a circle centered at the current state with a radius r . In this evaluation, we set the number of actions $Q = 12$ and the action radius as $r = 0.5m$. An action point can be viewed as the “carrot-dangling” waypoint for the robot to follow, which serves as the input to the low-level motion controller. For the reward function, we set the reward

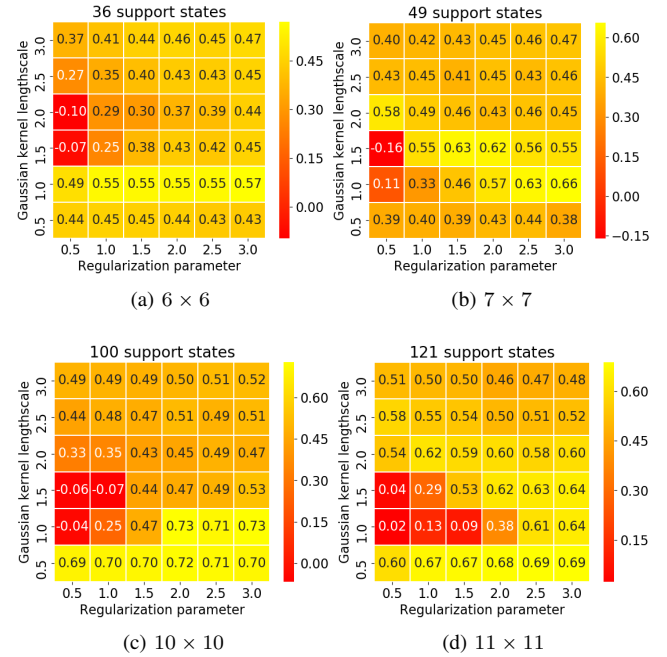


Fig. 4: The performance matrix obtained by the hyperparameter search using (a) 6×6 ; (b) 7×7 ; (c) 10×10 ; and (d) 11×11 evenly-spaced supporting states. Rows and columns represent different Gaussian kernel lengthscales and regularization parameters, respectively. The numbers in the color map represent the average return of the final policy obtained using the corresponding hyperparameter combination. The colorbar is shown on the right side of each table.

of arriving at the goal and obstacle states to be $+1$ and -1 , respectively. Since the reward now depends on the next state, we use Monte-carlo sampling to estimate the expectation of $R(s, a)$. The discount factor for the reward is set to $\gamma = 0.9$. We set the obstacle areas and the goal as absorbing states, i.e., the robot cannot transit to any other states if they are in these states. To satisfy the boundary condition mentioned in Section IV-B, we allow the robot to receive rewards at the

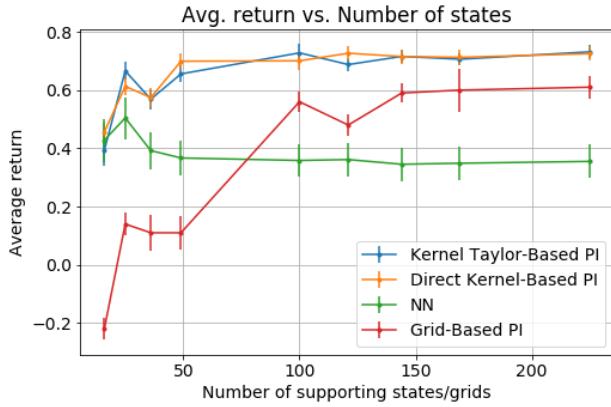


Fig. 5: The comparison of the average return of the policies computed from the four algorithms. The x-axis is the number of supporting states/grids used in computing the policy. The y-axis shows the average return.

goal state, but it cannot receive any reward if its current state is within an obstacle.

2) *Performance measure*:: Since the ultimate goal of planning is to find the optimal policy, our performance measure is based on the quality of the policy. A policy is better if it achieves a higher expected cumulative reward starting from every state. Because it is impossible to evaluate over an infinite number of states, we numerically evaluate the quality of a policy using the average return criterion [71]. In detail, we first uniformly sample $Q = 10^4$ states to ensure a thorough performance evaluation. Then, for each sampled state, we execute the policy for multiple trials, i.e., generating multiple trajectories, where each trajectory ends when it arrives at a terminal state (goal or obstacle) or reaches an allowable maximal number of steps. This procedure gives us an expected performance of the policy at any state by averaging the discounted sum of rewards over all the trajectories starting from it. Now, we can calculate the average return criterion by averaging over the performance of sampled states. A higher value of the average return implies that, on average, the policy gives better performance over the entire state space.

3) *Results*:: We are interested in examining the performance trends under varying supporting states and related parameters. To achieve this goal, we place evenly-spaced supporting states (in a lattice pattern) with different spacing resolution. Besides the number of states, the kernel length-scale and the regularization parameter λ are the other two hyperparameters governing the performance of our algorithm. We present the grid-based hyperparameter search results using four different configurations of supporting states shown in Fig. 4. The lengthscale and regularization parameters are searched over a set of values whose range is pre-estimated by the work-space dimensions and configurations, $\{0.5, 1, 1.5, 2, 2.5, 3\}$. By entry-wise comparison among the four matrices in Fig. 4, we can observe that increasing the number of states leads to improving performance in

general. However, we can find that the best performed policy is given by the 10×10 supporting states configuration (Fig. (c)) which is not the scenario with the best spacing resolution. This indicates that *a larger number of states can also result in a deteriorating solution*, and the performance of the algorithm is a matter of *how the supporting states are placed (distributed)*, instead of *the number (resolution) of state discretization*. Furthermore, we can gain some insights on how to select the hyperparameters based on the number of supporting states. Low-performing entries (highlighted with red) occur more often on the left side of the performance matrix when the number of supporting states increases. It implies that with more supporting states, the algorithm requires a stronger regularization (i.e., greater λ described in Section IV-C). On the other hand, high-performing policies (indicated by yellow) appear more on the bottom of the performance matrix when a greater number of supporting states present, which means that a smaller length scale is generally required given a larger quantity of supporting states.

We further compare our kernelized value function representation against other three variants of the value function approximations. Specifically, the first one is the direct kernel-based approximation method using a Gaussian kernel. This method is similar to the one in [24], but with a fully known transition function. The second one uses neural networks (NNs) as the value function approximator. We set up the NN configuration similar to a recent work [72]. In detail, we use a shallow two-layer network with 100 hidden units in each layer. Its parameters are optimized through minimizing the squared Bellman error via gradient descent. Since there is no closed-form solution to compute the expected next state value when using NN as a function approximator, we use Monte-Carlo sampling to estimate the expected value at the next states $\mathbb{E}[v^\pi(s')|s]$. The third method is the discrete grid-based approximation method. It first transforms the continuous MDP to a discrete version, where each state is regarded as a grid. Then, it uses the vanilla policy iteration to solve the discretized MDP.

The comparison among above methods aims at investigating two important questions:

- 1) How does the kernelized value function representation perform compared to other representations (NN and grid-based) in terms of the final policy performance?
- 2) Compared to our method, the direct kernel-based method not only requires the fully known transition function, but also restricts the transition to be a Gaussian distribution. Can our method with only mean and variance obtain similar performance as the direct kernel-based method?

To answer these questions, we choose the transition function as a Gaussian distribution. Its mean is the selected (intended) next waypoint. We set the standard deviation of the transition function to be $0.2m$ in both axes during the experiment. The transition probability models the accuracy of the low-level motion controller: more accurate controller leads to smaller

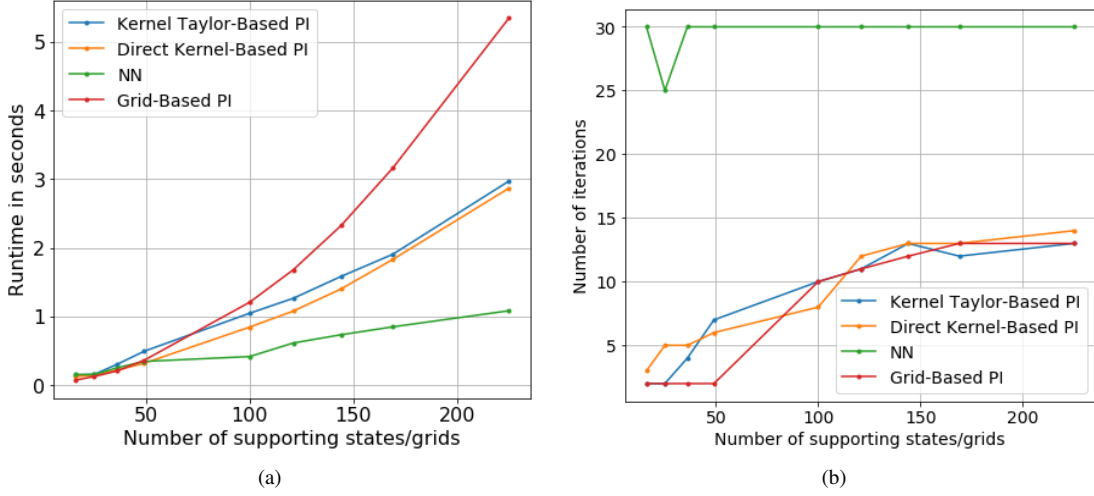


Fig. 6: Computational time comparisons of the four algorithms with changing number of states. (a) The computational time per iteration. (b) Number of iterations to convergence.

uncertainty. To perform fair comparisons, we use the same supporting states and apply hyperparameter search across all the methods.

The results for four methods are shown in Fig. 5 in terms of the average return. The first question is answered by the fact that the kernel-based methods (our kernel Taylor-based and the direct kernel-based PI) consistently outperform the other two methods. Moreover, our method has the performance as good as the direct kernel-based method which however requires the prerequisite full distribution information of the transition. This indicates that our method can be applied to broader applications that do not have full knowledge of transition functions. In contrast to the grid-based PI, the kernel-based algorithms and NN can achieve moderate performance even with a small number of supporting states. It implies that the continuous representation of the value function is crucial when supporting states are sparse. However, increasing the number of states does not improve the performance of the NN.

In Fig. 6, we compare the computational time and the number of iterations to convergence. The computational time of our method is less than the grid-based method as revealed in Fig. 6(a). We notice that there is a negligible computational time difference between our method and the direct method. As a parametric method, NN has the least computational time, and only linearly increases, but it does not converge as indicated by Fig. 6(b).

The function values and the final policies are visualized in Fig. 3. All the methods except for the NN obtain reasonable approximations to the optimal value function. Compared to our method, the values generated by the grid-based method are discrete “color blocks”, thus the obtained policy is non-smooth.

B. Martian Terrain Navigation

In this evaluation, we consider the autonomous navigation task on the surface of Mars with a rover. We obtain the Mars terrain data from *High Resolution Imaging Science Experiment* (HiRISE) [73]. Since there is no explicitly presented “obstacle”, the robot only receives the reward when it reaches the goal. If the rover attempts to move on a steep slope, it may be damaged and trapped within the same state with probability proportional to the slope angle. Otherwise, its next state is distributed around the desired waypoint following by the current action. This indicates that the underlying transition function should be the mixture of these two factors, and it is reasonable to assume that the means of the two cases are given by the current state and the next waypoint, respectively. We can similarly have an estimate of the variances. The mean and the variance of the transition function can then be computed using the law of total expectation and total variance, respectively.

Due to the complex and unstructured terrestrial features, evenly-spaced supporting state points may fail to best characterize the underlying value function. Also, to keep the computational time at a reasonable amount while maintaining a good performance, we leverage the importance sampling technique to sample the supporting states that concentrate around the dangerous regions where there are steep slopes. This is obtained by first drawing a large number of states uniformly covering the whole workspace. For each sampled state, we then assign a weight proportional to its slope angle. Finally, we resample supporting states based on the weights. To guarantee the goal state to have a value, we always place one supporting state at the center of the goal area.

Fig. 7(a) and Fig. 7(c) compare the two methods for supporting state selections. The supporting states given by the importance sampling-based method are dense around the slopes. These supporting states better characterize the potentially high-cost and dangerous areas than the evenly-

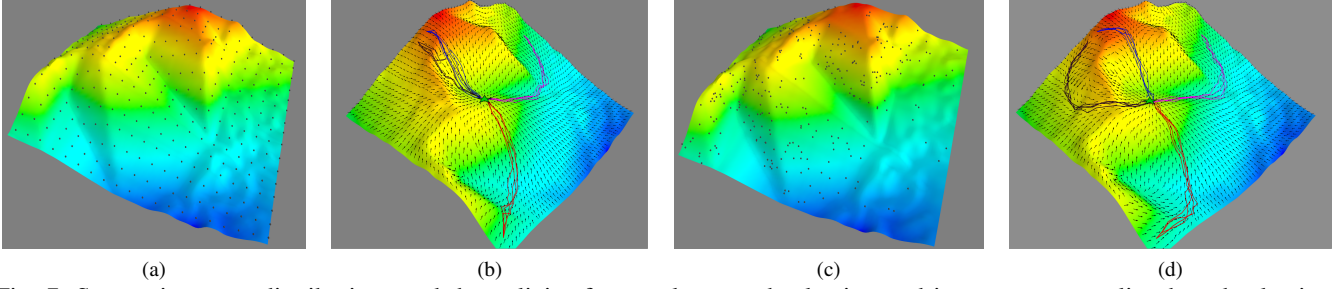


Fig. 7: Supporting state distributions and the policies for evenly-spaced selection and importance sampling-based selection. The 3D surface shows the Mars digital terrain model obtained from HiRISE. Supporting states and policies are shown in black dots and vector fields, respectively. The colored lines represent sampled trajectories, which initiate from four different starting positions. (a)(b) The evenly-spaced supporting states and the corresponding policy and trajectories; (c)(d) The supporting states generated by importance sampling and the corresponding policy and trajectories.

spaced selection scheme. We selected four starting locations from where the rover needs to plan paths to arrive at a goal location. For each starting location, we conducted multiple trials following the produced optimal policies. The trajectories generated with the importance sampling states in Fig. 7(d) attempt to approach the goal (green star) with minimum distances, and at the same time, avoid dangerous high-elevation terrains. In contrast, the trajectories obtained using the evenly-spacing states in Fig. 7(b) approach the goal in a more aggressive manner which can be risky in terms of safety. It indicates that a good selection of supporting states can better capture the state value function and thus produce finer solutions. This superior performance can also be reflected in Fig. 8(b). The policy obtained by the uniformly sampled states shows similar performance to the one generated by the evenly-spacing states, both of which yield smaller average return than the importance-sampled case. A top-down view of the policy is shown in Fig. 8(a) where the background color map denotes the elevation of terrain.

VI. AUTONOMY SYSTEM DESIGN

Previous algorithmic evaluations assume that a well-defined MDP can be abstracted and constructed from the real-world problem, and focus on algorithmic property/performance assessments. However, in reality, specifying an MDP for stochastic motion planning problems requires a known task region for constructing the state space as well as detailed information of the environment for transition and reward functions. These requirements are generally very difficult to satisfy if we deploy the robots into the real world, especially in the off-road environment where the task region is hard to define and no prior map is provided. In such cases, the robot needs to use its onboard sensors to acquire information and make decisions online. Specifically, it needs to process the observations, construct a new MDP within the observed area, compute the corresponding policy, and execute the policy. This process should repeat until the task is completed. In this paper, we only focus on generating a local policy within the observable area.

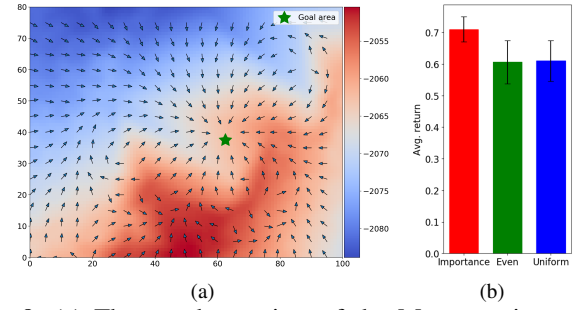


Fig. 8: (a) The top-down view of the Mars terrain surface as well as the policy generated by our method with the importance sampling selection. The color map indicates the height (in meters) of the terrain. (b) The comparison of average returns among three supporting state selection methods using the same number of states. Red, green, and blue bars indicate the performance of importance sampling selection, evenly-spaced selection, and uniform distribution sampling selection, respectively.

Note that, the global planning in any unknown environment might require information-driven (active) sensing to achieve a trade-off between the exploration of unknown space and the exploitation of observed space, which however is not the focus in this work. In this section, we present our autonomy system that extracts the MDP elements (supporting states, transition function, and reward function) from sensor data and connect the perception to the action loop. Fig. 9 provides an overview of the system.

A. Perception

The perception module is responsible for processing sensor observation and providing information for planning. It generates the robot state (pose) and a map of the environment in the field of view. The pose information can be estimated by any existing localization methods (e.g., [74]). The type of the map is important as it represents the information about what factors in the environment the robot needs to consider during planning. Because navigating on uneven ter-

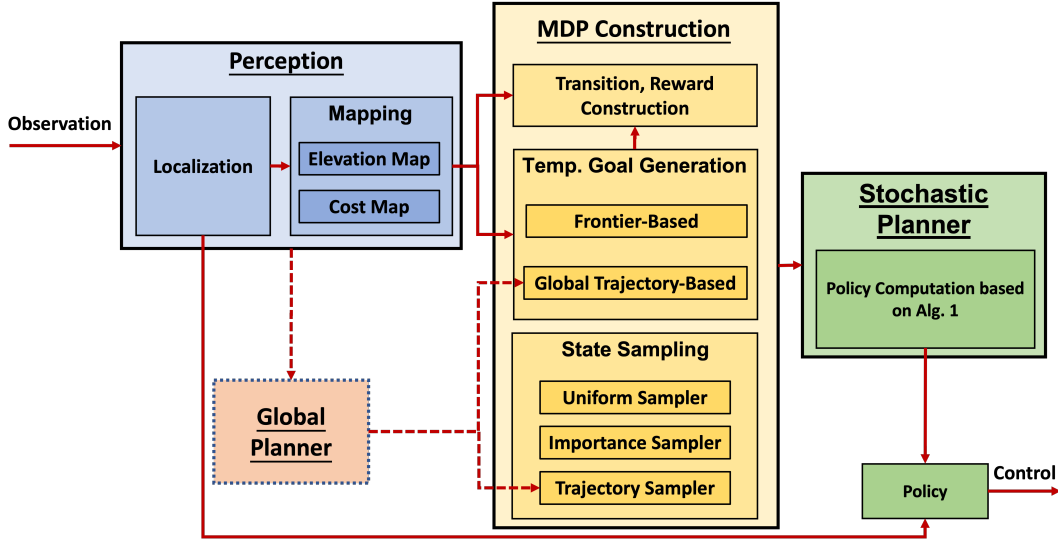


Fig. 9: An overview of the system for navigation in prior-unknown environments. The red arrows represent the direction of the information flow. The global planner module in the dashed block is optional.

rains requires both the occupancy information for identifying feasible regions and the elevation information for reasoning about the physical interaction between the robot and the terrain surface [75], we use a cost map computed from an occupancy map and an elevation map, or a combination of both to represent the environment.

B. MDP Construction

The second part of the system builds an MDP using the mapping information. In the following, we provide detailed explanations of this construction process for each MDP element.

1) *State and Action Spaces*:: The state and action spaces are pre-defined with the given vehicle type (ground). Specifically, the state is represented as the robot pose with position and orientation information (x, y, θ) , and the action consists of linear and angular speeds (v, ω) . Since our method deals with the discrete action space, we can tessellate the continuous action into evenly-spaced intervals. The discretization resolution, as well as the minimum and maximum values for the speeds, depend on the capability of the robot and the complexity of the task.

2) *Reward Function*:: The reward function consists of two parts $R(s) = (1 - \mathbb{I}_{s_g}(s))c(s) + r_g\mathbb{I}_{s_g}(s)$, where the first part $c(s)$ is the obstacle penalty provided by the cost map, $\mathbb{I}_{s_g}(s)$ is an indicator function for checking whether the state belongs to the goal region s_g , and r_g is the goal reward. If the cost map is not used, the obstacle penalty part is not included, and the robot only receives a positive reward if it arrives at the goal. Since we focus on planning within the observable space only, we need to generate a dummy goal region s_g in the space of the field of view. In other words, it needs to set a temporary goal if the final goal region is outside of the robot's current observed area. We use two heuristic approaches to generate this temporary goal. The first one is inspired by the frontier-based concept which

generates a temporary goal chosen at the boundary of the current observable map and with the least distance towards the final goal [76], [77]. The second method utilizes the path generated by a global planner if available (usually just for high level guidance). The temporary goal can be determined by "cropping" a path segment from the global path within the field of view only, where the path segment starts from the current robot pose and extends to a pre-defined length along the path, and the final pose on the extracted path segment serves as the temporary goal. Note that such a global planner is not mandatory for our method as it can be replaced with the frontier-based goal selection method.

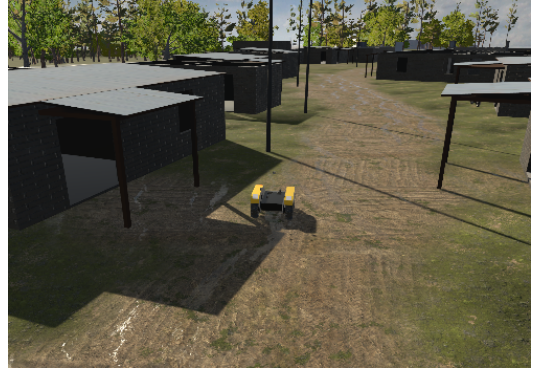
3) *First Two Moments of the Transition Function*:: We assume that the robot motion is generated based on $s' = f(s, a, h) + \epsilon$, where $f(s, a, h)$ is a deterministic function representing the discrete-time motion model related to vehicle dynamics, e.g., a differential drive model; $h(s)$ is the slope angle at state s derived from the elevation map; and ϵ is a noise term independent of the state and action. If the elevation map is used, the motion model considers the effect of the elevation on the robot's motion. Otherwise, we treat $h(s) = 0$ (flat surface) for all states in the current state space. To construct $f(s, a, h)$, we modify the Dubin's car model to take into consideration of the terrain slope, $x' = (\frac{\pi}{2} - h(s))(x + v\Delta t \cos \theta) + h(s)x$, $y' = (\frac{\pi}{2} - h(s))(y + v\Delta t \sin \theta) + h(s)y$, and $\theta' = \theta + \omega\Delta t$. Here, $h(s) \in [0, \frac{\pi}{2}]$ is the slope angle at state s and Δt is the time discretization resolution. Intuitively, this model penalizes the distance traveled on the surface with larger slope angle. Based on this formulation and Eq. (6), the first and second moments can be computed as $\mu(s, a, h) = \Delta_a s + \mathbb{E}[\epsilon]$ and $\sigma(s, a, h) = \mathbb{V}[\epsilon] + \mu(s, a, h)\mu(s, a, h)^T$, where $\Delta_a s = f(s, a, h) - s$ is the state shift after applying action a . The advantage of our method is obvious from the above modeling perspective. Since we only need to model

the mean and variance of the noise ϵ , it is not necessary to acquire the exact probability distribution of the noise.

4) *Supporting States*:: The last part of the construction is state sampling, which is responsible for distributing the supporting states within the state space. The positions and the number of the supporting states are critical as they determine the accuracy of the value function and also the computational time. More supporting states generally provide a better estimation of the optimal value function but require more time to compute as shown in Section V-A. We consider uniform sampling, importance sampling, and trajectory sampling strategies in this work. All these sampling methods require a region to distribute the supporting states. The first two methods introduced in Section V-A and Section V-B need prior knowledge of the environment and specifying a sampling region manually, e.g., a rectangular workspace. Uniform sampling tessellates a pre-defined region into equal-sized cells and uses the cell vertices as the supporting states. The importance sampler first uniformly samples a large number of states and then selects them based on some weighting criteria, e.g., the slope of the terrain at a given state point. The trajectory sampler utilizes the global path generated by a global planner as a heuristic to define the planning and sampling region. It distributes the state samples around the same path segment extracted from the global trajectory-based goal generation method. This method is especially useful when the fast online computation is required, since it does not need to search over the entire planning region.

C. Policy Execution

With all the MDP elements ready, we can use Alg. 1 to compute a policy for the constructed MDP. Then, this policy is used for generating control actions $a = (v, \omega) = \pi(s)$. It is necessary to discuss how this system can achieve online execution as this is important for local motion control. Most of the computation is spent on the policy iterations, which require $\mathcal{O}(|\mathbb{A}| \times |s|^2)$ for policy improvement (iterating over every action at every supporting state) and at most $\mathcal{O}(|s|^3)$ for policy evaluation (solving the linear system in Eq. (10)). Fortunately, once the policy is computed, it is relatively fast to obtain an action, because it only involves iterating over all the actions and searching for the best one at one state. Depending on the scenario, we provide two ways to perform online execution. In the first method, the policy computation and execution are separate: when the robot arrives at a temporary goal, it waits until the policy computation converges. Then, the robot carries out the newly computed policy. The benefit of this method lies in that since the policy computation process is separate from the subsequent online execution, it is suitable for those tasks needing sophisticated supporting state sampling schemes. However, this separation may cause the robot to have a discontinuous behavior with periodical pauses. The second method uses an MPC-based idea by combining policy computation and execution into one process. At each time step (when the robot takes an action), we construct a new MDP and computes the corresponding policy. Then the robot only takes one action from the policy



(a) A snapshot of the simulator



(b) The top-down view of the environment

Fig. 10: A snapshot and the top-down view of the high fidelity simulator

and repeats the computation. This method is suitable for the task where a small number of supporting states is enough to ensure online computation and safe maneuver. Thus, practically one can combine this online execution with the trajectory sampling, where a global planner can provide a heuristic for the supporting state selection.

VII. SIMULATION WITH LiDAR PERCEPTION

To accomplish the off-road navigation autonomy system described above, we first integrate the perception module and also test the system performance. In this way, the robot is no longer provided with a prior map of the environment, and it can observe the environment and obtain state information from its onboard LiDAR.

The testing scenario is to navigate the robot safely without a prior map in a cluttered outdoor environment that contains buildings and random obstacles. Fig. 10 shows a snapshot of the simulator and a bird-eye view of the simulated environment. The simulator simulates a ClearPath Warthog differential drive ground vehicle equipped with a 64-beam LiDAR. We set the robot's minimum and maximum values for linear and angular speeds as $v_{min} = -1m/s$, $v_{max} = 3m/s$, $\omega_{min} = -1.5rad/s$ (turning right), and $\omega_{max} = 1.5rad/s$ (turning left). We consider a task where the robot needs to arrive at a set of pre-defined waypoints sequentially and return back to the initial position. We define three levels of difficulties: easy, medium, hard. The difficulty level increases as the number of waypoints decreases. This is

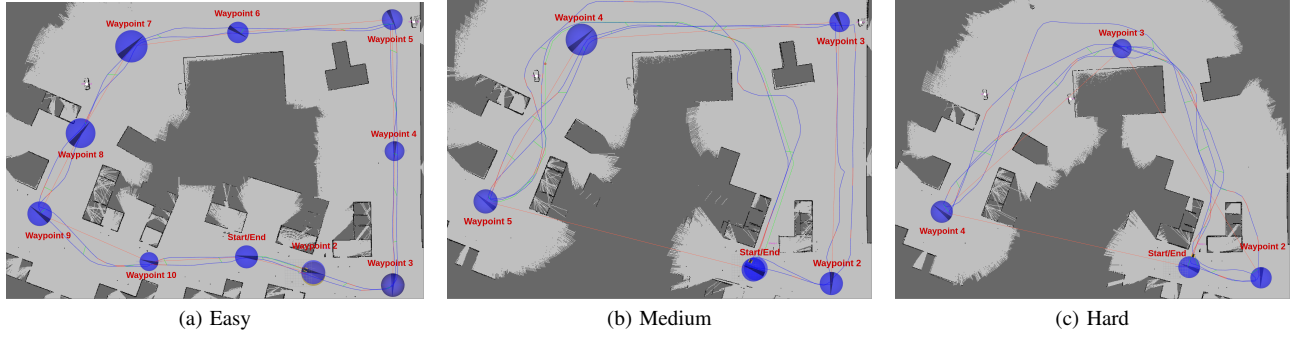


Fig. 11: The mission maps and sampled robot trajectories for each difficulty level. The blue circles are the waypoints. The number of waypoints decreases as the difficulty increases (from left to right). For each difficulty level, the robot starts from the initial position, navigates sequentially to the next points, and returns to the initial position. Two sampled robot trajectories for our method are shown in blue lines.

because the robot receives less guidance and needs to make more decisions on its own. Fig. 11 shows the waypoint positions, the constructed cost map, and two sampled trajectories for each difficulty level using our method.

We compare our method with a baseline local planner, nonlinear model predictive control (NMPC) [78], which generally represents a set of conventional, motion primitive-based planning algorithms from literature and has demonstrated great applicability in real-world environments [79]. This deterministic planner produces smooth trajectories that respect the robot’s dynamics by optimizing a cost function that penalizes the path deviation from a desired global trajectory using algorithms from the NLOPT library [80]. Here, an anytime version of A* (ARA*) [81] is employed as the global planner to provide the desired reference trajectory and a PID tracking controller is used to execute the optimized path. This pipeline is often adopted by the traditional three-layer planning and control system. To make a fair comparison, we also leverage the global planner to generate temporary goal points and sampling supporting states, which are mentioned in Section VI. In this experiment, we choose $6m$ as the length of trajectory sampling, which means that the robot plans $2s$ in the future if it uses the maximum speed (which is $3m/s$). For our method, the actions are discretized evenly into 8×8 intervals which are dense enough to approximate continuous actions.

We use completion time and averaged linear velocities as the performance metrics. The completion time is the total travel time for finishing the task, and the smaller the better. The averaged velocities reflect the motion smoothness of the robot (within speed limit) and thus the larger the better. Compared to the averaged cumulative rewards, these metrics are more relevant to the robot navigation task. The result is shown in Fig. 12. In general, our method is more efficient and can complete the task in a shorter time as shown in Fig. 12(a). Since the NMPC method attempts to follow the global path exactly, the trajectory optimized by NMPC sometimes oscillates around and overshoots the global path. This oscillation causes the vehicle to reduce its speed due to

frequent turning. In contrast, since our method considers the uncertainty (via the second moment) of the robot’s motion, it can reason over some areal coverage around the global path. As a result, as long as the robot remains within the area supported by the sampled states, it does not show the oscillation behavior. We can also observe this result from Fig. 12(b) where our method’s average velocity is larger than the NMPC approach.

It is also worth pointing that, the robot uses a shorter time to complete the task in the hard mission than in the easy one, but the linear velocity in the hard mission is smaller than the one in the easy mission. This can be explained by observing the trajectories the robot generated in the two missions in Fig. 11. Although the easy mission provides denser waypoints, the robot is restricted to follow these predefined points which are not necessarily the shortest route. In contrast, the hard mission’s waypoints are sparse and thus the mission has less restriction on which trajectory the robot should follow. As a result, the robot chooses a shortcut to navigate from Waypoint 2 to Waypoint 3 as shown in Fig. 11(c).

VIII. REAL-WORLD DEMONSTRATIONS IN INDOOR CLUTTERED AND OUTDOOR UNSTRUCTURED ENVIRONMENTS

To demonstrate the applicability of our system in the real world, we conducted extensive real-world trials in different scenarios. The goal is to validate whether the proposed method can be used to generate effective policies that navigate a ground vehicle in complex and unstructured environments. The robot behaviors can be seen in video <https://youtu.be/6Xc8s4Bongg>.

A. Hardware Setup

We implement our system on two ground vehicles, ClearPath Jackal and Husky. Since Jackal is small in dimension and has a small wheel traction, it is only used for indoor experiment. It is equipped with a 16-beam Velodyne LiDAR for localization and mapping, a quad-core 2.7GHz CPU and

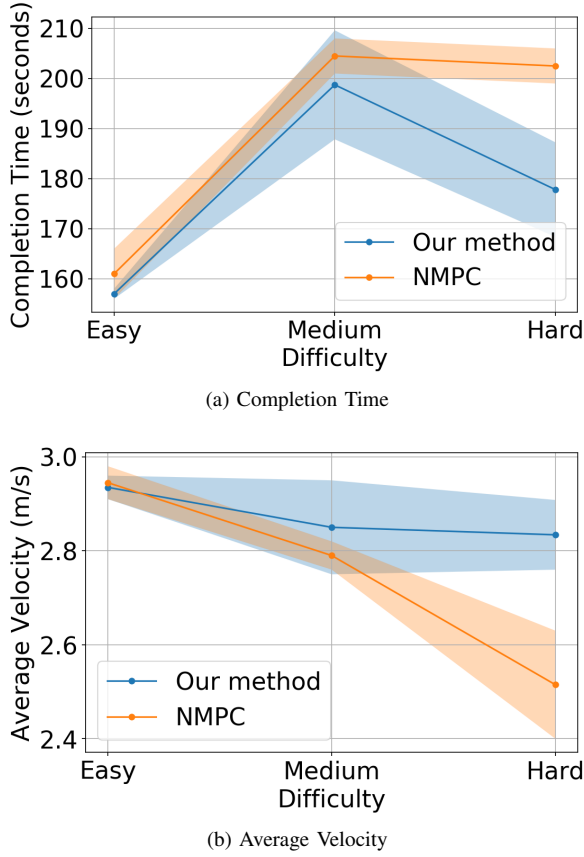


Fig. 12: Performance comparison between our method and NMPC. (a) and (b) show the time of task completion and the velocity averaged over the task. For both figures, the x -axis indicates the difficulty level. All the experiments are averaged over 10 trials.

16GB RAM for the onboard computation. Husky is used for navigating in outdoor environments, because it is larger in size and provides more traction when moving on rough terrains. Husky is equipped with a 64-beam Ouster LiDAR for more detailed terrain mapping and a Lord Microstrain 3DM-GX4-25 IMU for more accurate localization outdoor. It has an eight-core 2.7GHz Intel I7 CPU and 64GB RAM for the onboard computation.

B. Indoor Cluttered Environment

The setup is an indoor $5m \times 5m$ environment with random boxes as obstacles, and the task is to navigate the ClearPath Jackal to a goal location and return to the start position. The first aim is to validate the basic obstacle avoidance behavior in a prior unknown environment. The second aim is to demonstrate that our system can achieve efficient navigation behavior without a global planner, as well as use only the elevation map representation to construct the MDP and specify only a positive goal reward. Traditionally, the obstacle penalty in the reward (or cost) function is a proxy for indirectly expressing the consequence of collisions. With the elevation map representation, the transition function can

directly approximate how the environment’s geometry (in our case, elevation) affects robot’s motion, which includes the result of colliding with obstacles. This is because we formulate the transition function to penalize the distance traveled on high-slope surfaces as mentioned, and obstacles generally have large slope angles.

Since the planning region in this case is observable and can be pre-specified¹, i.e., a $5m \times 5m$ square, we can evenly distribute 6 supporting states in each of the x, y dimensions, so that the distance between two neighboring states is $1m$ in each dimension. However, because it is difficult to predict what heading angles the robot may take during the task execution, we need supporting states to cover one full rotation of the heading angle, i.e., $[-\pi, \pi)$. Specifically, we place 10 equidistant states in the θ dimension, so that the distance between two neighboring states along the θ dimension is $\frac{\pi}{5}$. The total number of states is 360.

The range of linear and angular speeds are set to $v \in [-0.5m/s, 1.5m/s]$ and $\omega \in [-1.5rad/s, 1.5rad/s]$, respectively. The environment, a sequence of the robot’s snapshots, and detailed planning information are shown in Fig. 13. The initial position of the robot is placed in front of the obstacles, and the goal is between the two obstacles and is indicated by the green square on the second row of Fig. 13. Initially, due to the occlusion by randomly placed boxes, the robot can only build a partial elevation map using the observed points. Then, it uses this initial map to calculate the value function within the $5m \times 5m$ squared region. The value function is shown as the upper $2.5D$ surface in the second row. To aid the visualization, we only draw the value function over the position variables at the current robot’s angle, and the height of the surface represents the state value. We can observe that the value function correctly characterizes the geometry of the environment and the task. Specifically, the goal region has the highest state value. Since the policy always selects actions that maximize the state value, executing the policy from this value function will allow the robot to converge at the goal point. Additionally, on the value function surface, the narrow ridge between the two obstacles reflects the navigable space correctly. Thus, the resulting policy can navigate through the passage safely as shown in the first row of Fig. 13. As the robot executes its planned policy, it receives more sensing points and gradually builds a more detailed elevation map. We can see this process from the second and fourth rows. After the robot arrives at the goal, it re-plans and returns to the initial position, which is shown in the third row. We can observe that the computed value function allows the robot to reason about its nonholonomic motion through the transition function. Since the forward velocity is larger than the backward velocity, the robot reverses and turns to align its forward axis to the initial position to ensure it uses the maximum speed. This also reveals that our method exhibits a *speed-adaptive* behavior for the most efficient motion.

¹Note that it does not mean that the environment map is provided a-prior.

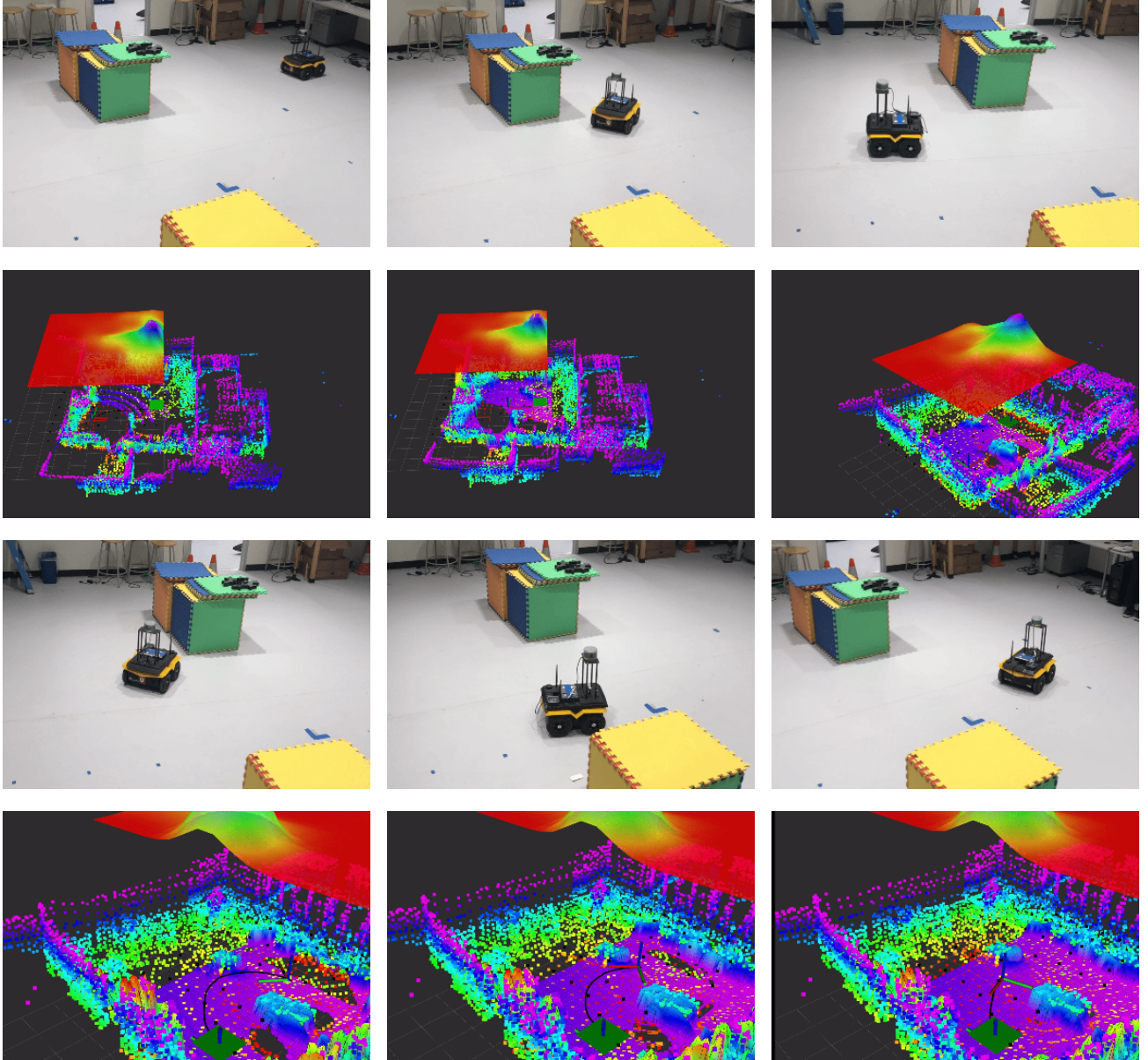


Fig. 13: The indoor environment where our method is tested for validating its basic obstacle-avoidance behavior. The first and third rows show the vehicles' behavior at different timesteps, and the second and fourth rows depict the corresponding visualization results. The task for the robot is to navigate through the gap between boxes (approximately $1.5m$) and arrive at the green square shown in the second row, and then return back to the initial position. The colored dots are the point cloud generated from the LiDAR sensing. Upper and lower $2.5D$ color maps represent the value function and the elevation map, respectively. The height of the value function represents the state value. The planned expected trajectory is shown in black curves. The axes represent the pose of the robot.

C. Outdoor Unstructured Environment

We further test our system in two types of outdoor environments shown in Fig. 14 and Fig. 15. These environments are used to test our method's performance in more complex and unstructured environments.

Fig. 14 demonstrates the snapshots of the robot navigating on a terrain that has varying elevations. This environment contains a dune with a maximum height of approximately

$1.0m$, a high slope in the middle, and a low slope surface to the left of the robot's initial position. In this environment, we use elevation map and importance sampling to construct the MDP, where the weight is given by the slope angle. The robot's initial pose directly faces the part of the terrain that has the highest slope angle. The goal is placed behind the sand dune indicated as a red circle in the second row of Fig. 14. The shortest path between the robot's initial pose

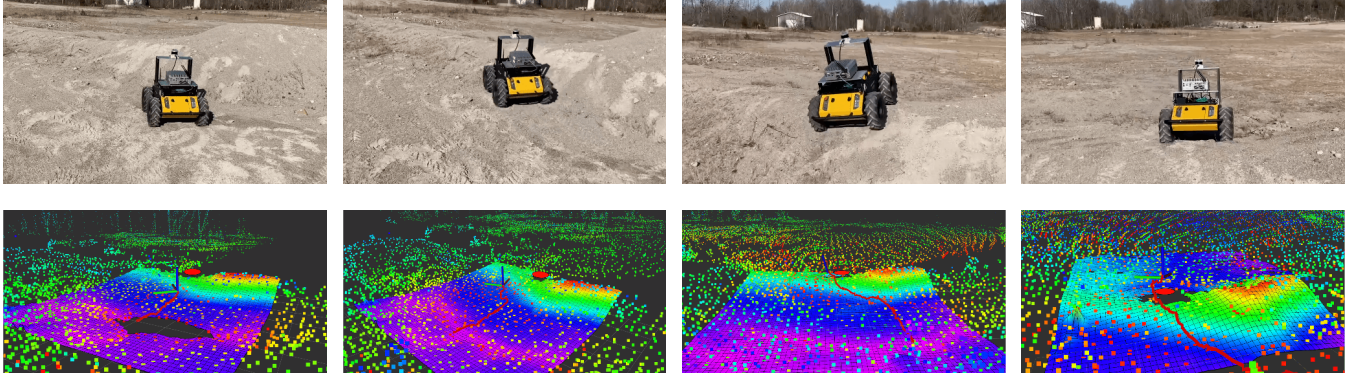


Fig. 14: Snapshots of navigating in the elevation-rich environment. The two rows show the real system and the visualization, respectively. The traversed trajectories and goals are shown in red curves and red circles.

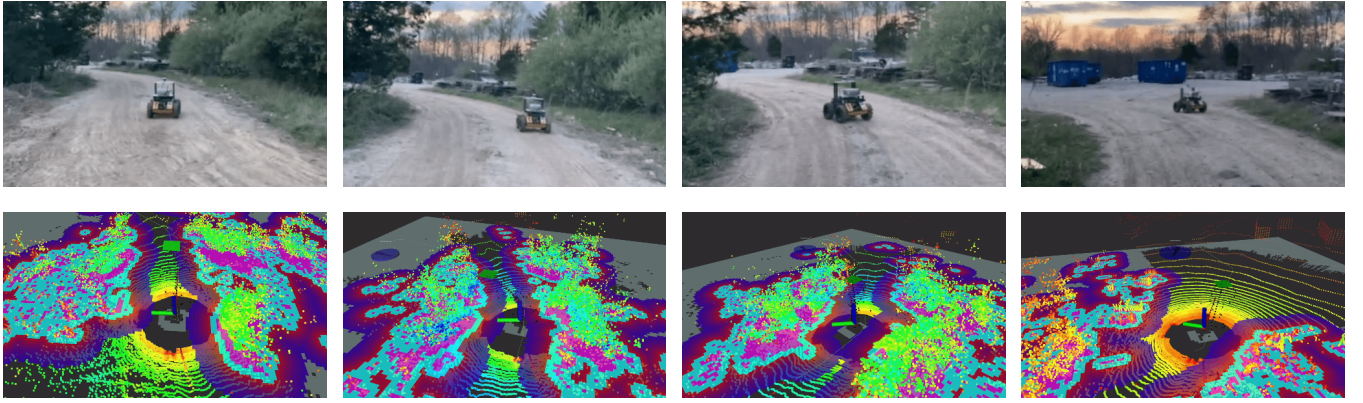


Fig. 15: Snapshots of navigation in a trail using trajectory sampling to sample the states and cost map to represent the environment. The visualization in the second row shows the cost map as a 2D color map, where a darker color means larger cost. The red trajectory represents the expected path by executing the policy, and the black dots around the green global trajectory are the sampled states. The goal for each time step is shown as a green square. The final goal is the blue circle.

and the goal is a straight line crossing the up-slope terrain, but it is difficult (and dangerous) for the vehicle to traverse. We can observe in the first three columns of Fig. 14 that the robot takes safe maneuver to avoid the dangerous terrain. This is because we penalize the robot’s movement distance on high slope surfaces, the resulting policy can guide the robot to avoid the dune. The last column shows that after arriving at the current goal, the vehicle extends its elevation map, updates the MDP, and computes a new policy.

Fig. 15 shows the robot navigating on a trail surrounded by various vegetation. Since this environment does not contain elevated terrains, it is only necessary to provide obstacle penalty using a cost map. As described in Section VII, we use trajectory-based supporting state sampling and goal generation for fast traversal in this scenario. The figure shows that our system allows the robot to navigate through the trail safely without colliding into the dense vegetation and other obstacles.

IX. CONCLUSION AND DISCUSSION

This paper presents a new decision making framework for robot planning and control in complex and unstructured environments such as the off-road navigation. We propose a method to solve the continuous-state Markov Decision Process by integrating the kernel value function representation and the Taylor-based approximation to Bellman optimality equation. Our algorithm alleviates the need for heavily searching in continuous state space and the need for precisely modeling the state transition functions. We have validated the proposed method through thorough evaluations in both simplified and realistic planning scenarios. The experiments comparing with other baseline approaches show that our proposed framework is powerful and flexible, and the performance statistics reveal superior efficiency and accuracy of the presented algorithm.

In addition to the theoretical contribution, our real-world experiments reveal several challenges of applying the proposed method in practice. We present a system (Section VI) which is mainly responsible for converting the raw sensor

data to an MDP problem by assuming that feasible/infeasible regions can be distinguished and the features in the environment (elevation in our experiment) can be obtained accurately from sensors. Since this MDP is used for computing a policy, ensuring the MDP matches the real-world scenario is paramount in the final performance of the system. However, the map built from the noisy sensor measurement usually cannot accurately represent the geometry of the environment, e.g., occupancy and elevation. The MDP derived from this inaccurate map may deviate from the real environment. Thus, reasoning about these inaccuracies in the planning method is essential for building a robust navigation system. Additionally, an accurate physics model for planning is necessary in complex environments, where detailed motion control strategies are needed. By comparing the results of the Section V-A and Section VIII, we can observe that the planning method can generate more efficient policies if we use a physics model which can better describe the robot's motion. In our real-world experiments, our modeling of the first moment uses inaccurate models to describe the physical interaction between the robot and the terrain. Although these models can be used for planning in the particular environments we tested, to generalize to more complex situations, it is necessary to develop more accurate physical models that consider not only the elevation but also terrain textures, which is our future work.

ACKNOWLEDGEMENT

This research was supported by the Army Research Office with grant number W911NF-20-2-0099, the National Science Foundation with grant number 2006886, and an Amazon Research Award.

REFERENCES

- [1] C. Boutilier, T. Dean, and S. Hanks, "Decision-theoretic planning: Structural assumptions and computational leverage," *Journal of Artificial Intelligence Research*, vol. 11, pp. 1–94, 1999.
- [2] S. Thrun, W. Burgard, and D. Fox, *Probabilistic robotics*. MIT press Cambridge, 2000, vol. 1.
- [3] J. Kober, J. A. Bagnell, and J. Peters, "Reinforcement learning in robotics: A survey," *The International Journal of Robotics Research*, vol. 32, no. 11, pp. 1238–1274, 2013.
- [4] D. P. Bertsekas, *Dynamic programming and optimal control*. Athena scientific Belmont, MA, 1995, vol. 1, no. 2.
- [5] R. S. Sutton and A. G. Barto, *Reinforcement learning: An introduction*. MIT press, 2018.
- [6] A. A. Pereira, J. Binney, G. A. Hollinger, and G. S. Sukhatme, "Risk-aware path planning for autonomous underwater vehicles using predictive ocean models," *Journal of Field Robotics*, vol. 30, no. 5, pp. 741–762, 2013.
- [7] M. Otte, W. Silva, and E. Frew, "Any-time path-planning: Time-varying wind field+ moving obstacles," in *2016 IEEE International Conference on Robotics and Automation (ICRA)*. IEEE, 2016, pp. 2575–2582.
- [8] Y. Fu, X. Yu, and Y. Zhang, "Sense and collision avoidance of unmanned aerial vehicles using markov decision process and flatness approach," in *2015 IEEE International Conference on Information and Automation*. IEEE, 2015, pp. 714–719.
- [9] W. H. Al-Sabban, L. F. Gonzalez, and R. N. Smith, "Wind-energy based path planning for unmanned aerial vehicles using markov decision processes," in *2013 IEEE International Conference on Robotics and Automation (ICRA)*. IEEE, 2013, pp. 784–789.
- [10] S. S. Baek, H. Kwon, J. A. Yoder, and D. Pack, "Optimal path planning of a target-following fixed-wing uav using sequential decision processes," in *2013 IEEE/RSJ International Conference on Intelligent Robots and Systems*. IEEE, 2013, pp. 2955–2962.
- [11] R. E. Bellman, *Adaptive control processes: a guided tour*. Princeton university press, 2015, vol. 2045.
- [12] A. A. Gorodetsky, S. Karaman, and Y. M. Marzouk, "Efficient high-dimensional stochastic optimal motion control using tensor-train decomposition," in *Robotics: Science and Systems*, 2015.
- [13] L. Liu and G. S. Sukhatme, "A solution to time-varying markov decision processes," *IEEE Robotics and Automation Letters*, vol. 3, no. 3, pp. 1631–1638, 2018.
- [14] J. Xu, K. Yin, and L. Liu, "Reachable space characterization of markov decision processes with time variability," in *Proceedings of Robotics: Science and Systems*, Freiburg/Breisgau, Germany, June 2019.
- [15] R. Munos and A. Moore, "Variable resolution discretization in optimal control," *Machine learning*, vol. 49, no. 2-3, pp. 291–323, 2002.
- [16] S. M. LaValle, *Planning algorithms*. Cambridge university press, 2006.
- [17] D. P. Bertsekas and J. N. Tsitsiklis, *Neuro-dynamic programming*. Athena Scientific Belmont, MA, 1996, vol. 5.
- [18] R. Munos and C. Szepesvári, "Finite-time bounds for fitted value iteration," *Journal of Machine Learning Research*, vol. 9, no. May, pp. 815–857, 2008.
- [19] A. Antos, C. Szepesvári, and R. Munos, "Learning near-optimal policies with bellman-residual minimization based fitted policy iteration and a single sample path," *Machine Learning*, vol. 71, no. 1, pp. 89–129, 2008.
- [20] T. Hofmann, B. Schölkopf, and A. J. Smola, "Kernel methods in machine learning," *The annals of statistics*, pp. 1171–1220, 2008.
- [21] J. Shawe-Taylor, N. Cristianini *et al.*, *Kernel methods for pattern analysis*. Cambridge university press, 2004.
- [22] M. P. Deisenroth, C. E. Rasmussen, and J. Peters, "Gaussian process dynamic programming," *Neurocomputing*, vol. 72, no. 7-9, pp. 1508–1524, 2009.
- [23] Y. Engel, S. Mannor, and R. Meir, "Bayes meets bellman: The gaussian process approach to temporal difference learning," in *Proceedings of the 20th International Conference on Machine Learning (ICML-03)*, 2003, pp. 154–161.
- [24] M. Kuss and C. E. Rasmussen, "Gaussian processes in reinforcement learning," in *Advances in Neural Information Processing Systems*, 2004, pp. 751–758.
- [25] G. Taylor and R. Parr, "Kernelized value function approximation for reinforcement learning," in *Proceedings of the 26th Annual International Conference on Machine Learning*, 2009, pp. 1017–1024.
- [26] X. Xu, D. Hu, and X. Lu, "Kernel-based least squares policy iteration for reinforcement learning," *IEEE Transactions on Neural Networks*, vol. 18, no. 4, pp. 973–992, 2007.
- [27] J. Martin, J. Wang, and B. Englot, "Sparse gaussian process temporal difference learning for marine robot navigation," *arXiv preprint arXiv:1810.01217*, 2018.
- [28] K. Arulkumaran, M. P. Deisenroth, M. Brundage, and A. A. Bharath, "A brief survey of deep reinforcement learning," *arXiv preprint arXiv:1708.05866*, 2017.
- [29] X. Glorot and Y. Bengio, "Understanding the difficulty of training deep feedforward neural networks," in *Proceedings of the Thirteenth International Conference on Artificial Intelligence and Statistics*, 2010, pp. 249–256.
- [30] J. D. Gammell and M. P. Strub, "Asymptotically optimal sampling-based motion planning methods," *Annual Review of Control, Robotics, and Autonomous Systems*, vol. 4.
- [31] S. Karaman and E. Frazzoli, "Sampling-based algorithms for optimal motion planning," *The international journal of robotics research*, vol. 30, no. 7, pp. 846–894, 2011.
- [32] D. J. Webb and J. v. d. Berg, "Kinodynamic rrt*: Optimal motion planning for systems with linear differential constraints," *arXiv preprint arXiv:1205.5088*, 2012.
- [33] D. Mellinger and V. Kumar, "Minimum snap trajectory generation and control for quadrotors," in *2011 IEEE international conference on robotics and automation*. IEEE, 2011, pp. 2520–2525.
- [34] C. Richter, A. Bry, and N. Roy, "Polynomial trajectory planning for aggressive quadrotor flight in dense indoor environments," in *Robotics research*. Springer, 2016, pp. 649–666.
- [35] J. Chen, K. Su, and S. Shen, "Real-time safe trajectory generation for quadrotor flight in cluttered environments," in *2015 IEEE International*

- Conference on Robotics and Biomimetics (ROBIO)*. IEEE, 2015, pp. 1678–1685.
- [36] F. Gao, W. Wu, Y. Lin, and S. Shen, “Online safe trajectory generation for quadrotors using fast marching method and bernstein basis polynomial,” in *2018 IEEE International Conference on Robotics and Automation (ICRA)*. IEEE, 2018, pp. 344–351.
- [37] F. Gao and S. Shen, “Online quadrotor trajectory generation and autonomous navigation on point clouds,” in *2016 IEEE International Symposium on Safety, Security, and Rescue Robotics (SSRR)*. IEEE, 2016, pp. 139–146.
- [38] F. Gao, W. Wu, W. Gao, and S. Shen, “Flying on point clouds: Online trajectory generation and autonomous navigation for quadrotors in cluttered environments,” *Journal of Field Robotics*, vol. 36, no. 4, pp. 710–733, 2019.
- [39] S. Liu, M. Watterson, K. Mohta, K. Sun, S. Bhattacharya, C. J. Taylor, and V. Kumar, “Planning dynamically feasible trajectories for quadrotors using safe flight corridors in 3-d complex environments,” *IEEE Robotics and Automation Letters*, vol. 2, no. 3, pp. 1688–1695, 2017.
- [40] R. Deits and R. Tedrake, “Efficient mixed-integer planning for uavs in cluttered environments,” in *2015 IEEE international conference on robotics and automation (ICRA)*. IEEE, 2015, pp. 42–49.
- [41] B. Zhou, F. Gao, J. Pan, and S. Shen, “Robust real-time uav replanning using guided gradient-based optimization and topological paths,” in *2020 IEEE International Conference on Robotics and Automation (ICRA)*. IEEE, 2020, pp. 1208–1214.
- [42] H. Oleynikova, M. Burri, Z. Taylor, J. Nieto, R. Siegwart, and E. Galceran, “Continuous-time trajectory optimization for online uav replanning,” in *2016 IEEE/RSJ international conference on intelligent robots and systems (IROS)*. IEEE, 2016, pp. 5332–5339.
- [43] B. Zhou, F. Gao, L. Wang, C. Liu, and S. Shen, “Robust and efficient quadrotor trajectory generation for fast autonomous flight,” *IEEE Robotics and Automation Letters*, vol. 4, no. 4, pp. 3529–3536, 2019.
- [44] R. Tedrake, I. R. Manchester, M. Tobenkin, and J. W. Roberts, “Lqr-trees: Feedback motion planning via sums-of-squares verification,” *The International Journal of Robotics Research*, vol. 29, no. 8, pp. 1038–1052, 2010.
- [45] A.-A. Agha-Mohammadi, S. Chakravorty, and N. M. Amato, “Firm: Sampling-based feedback motion-planning under motion uncertainty and imperfect measurements,” *The International Journal of Robotics Research*, vol. 33, no. 2, pp. 268–304, 2014.
- [46] R. E. Kalman *et al.*, “Contributions to the theory of optimal control,” *Bol. soc. mat. mexicana*, vol. 5, no. 2, pp. 102–119, 1960.
- [47] J. Van Den Berg, P. Abbeel, and K. Goldberg, “Lqg-mp: Optimized path planning for robots with motion uncertainty and imperfect state information,” *The International Journal of Robotics Research*, vol. 30, no. 7, pp. 895–913, 2011.
- [48] V. A. Huynh, S. Karaman, and E. Frazzoli, “An incremental sampling-based algorithm for stochastic optimal control,” *The International Journal of Robotics Research*, vol. 35, no. 4, pp. 305–333, 2016.
- [49] J. B. Rawlings, D. Q. Mayne, and M. Diehl, *Model predictive control: theory, computation, and design*. Nob Hill Publishing Madison, WI, 2017, vol. 2.
- [50] D. P. Bertsekas, “Dynamic programming and suboptimal control: A survey from adp to mpc,” *European Journal of Control*, vol. 11, no. 4-5, pp. 310–334, 2005.
- [51] D. Bertsekas, *Dynamic programming and optimal control: Volume I*. Athena scientific, 2012, vol. 1.
- [52] A. Bemporad and M. Morari, “Robust model predictive control: A survey,” in *Robustness in identification and control*. Springer, 1999, pp. 207–226.
- [53] W. Langson, I. Chrysoschoos, S. Raković, and D. Q. Mayne, “Robust model predictive control using tubes,” *Automatica*, vol. 40, no. 1, pp. 125–133, 2004.
- [54] A. Majumdar and R. Tedrake, “Robust online motion planning with regions of finite time invariance,” in *Algorithmic foundations of robotics X*. Springer, 2013, pp. 543–558.
- [55] —, “Funnel libraries for real-time robust feedback motion planning,” *The International Journal of Robotics Research*, vol. 36, no. 8, pp. 947–982, 2017.
- [56] M. Althoff, O. Stursberg, and M. Buss, “Reachability analysis of nonlinear systems with uncertain parameters using conservative linearization,” in *2008 47th IEEE Conference on Decision and Control*. IEEE, 2008, pp. 4042–4048.
- [57] S. Bansal, M. Chen, S. Herbert, and C. J. Tomlin, “Hamilton-jacobi reachability: A brief overview and recent advances,” in *2017 IEEE 56th Annual Conference on Decision and Control (CDC)*. IEEE, 2017, pp. 2242–2253.
- [58] H. J. Kappen, V. Gómez, and M. Opper, “Optimal control as a graphical model inference problem,” *Machine learning*, vol. 87, no. 2, pp. 159–182, 2012.
- [59] E. Theodorou, J. Buchli, and S. Schaal, “A generalized path integral control approach to reinforcement learning,” *The Journal of Machine Learning Research*, vol. 11, pp. 3137–3181, 2010.
- [60] G. Williams, N. Wagener, B. Goldfain, P. Drews, J. M. Rehg, B. Boots, and E. A. Theodorou, “Information theoretic mpc for model-based reinforcement learning,” in *2017 IEEE International Conference on Robotics and Automation (ICRA)*. IEEE, 2017, pp. 1714–1721.
- [61] G. Williams, B. Goldfain, P. Drews, K. Saigol, J. M. Rehg, and E. A. Theodorou, “Robust sampling based model predictive control with sparse objective information,” in *Robotics: Science and Systems*, 2018.
- [62] W. B. Powell, “Perspectives of approximate dynamic programming,” *Annals of Operations Research*, vol. 241, no. 1-2, pp. 319–356, 2016.
- [63] G. J. Gordon, “Approximate solutions to markov decision processes,” Carnegie-Mellon University School of Computer Science, Tech. Rep., 1999.
- [64] D. P. Bertsekas, “Approximate policy iteration: A survey and some new methods,” *Journal of Control Theory and Applications*, vol. 9, no. 3, pp. 310–335, 2011.
- [65] M. L. Puterman, *Markov decision processes: discrete stochastic dynamic programming*. John Wiley & Sons, 2014.
- [66] M. G. Lagoudakis and R. Parr, “Least-squares policy iteration,” *Journal of machine learning research*, vol. 4, no. Dec, pp. 1107–1149, 2003.
- [67] A. Braverman, I. Gurvich, and J. Huang, “On the taylor expansion of value functions,” *Operations Research*, vol. 68, no. 2, pp. 631–654, 2020.
- [68] L. C. Evans, *Partial Differential Equations: Second Edition (Graduate Series in Mathematics)*. American Mathematical Society, 2010.
- [69] J. Si, A. G. Barto, W. B. Powell, and D. Wunsch, *Handbook of learning and approximate dynamic programming*. John Wiley & Sons, 2004, vol. 2.
- [70] M. Maurette, “Mars rover autonomous navigation,” *Autonomous Robots*, vol. 14, no. 2-3, pp. 199–208, 2003.
- [71] R. Islam, P. Henderson, M. Gomrokchi, and D. Precup, “Reproducibility of benchmarked deep reinforcement learning tasks for continuous control,” *arXiv preprint arXiv:1708.04133*, 2017.
- [72] N. Heess, G. Wayne, D. Silver, T. Lillicrap, T. Erez, and Y. Tassa, “Learning continuous control policies by stochastic value gradients,” in *Advances in Neural Information Processing Systems*, 2015, pp. 2944–2952.
- [73] A. S. McEwen, E. M. Eliason, J. W. Bergstrom, N. T. Bridges, C. J. Hansen, W. A. Delamere, J. A. Grant, V. C. Gulick, K. E. Herkenhoff, L. Keszthelyi *et al.*, “Mars reconnaissance orbiter’s high resolution imaging science experiment (hirise),” *Journal of Geophysical Research: Planets*, vol. 112, no. E5, 2007.
- [74] G. Bresson, Z. Alsayed, L. Yu, and S. Glaser, “Simultaneous localization and mapping: A survey of current trends in autonomous driving,” *IEEE Transactions on Intelligent Vehicles*, vol. 2, no. 3, pp. 194–220, 2017.
- [75] P. Fankhauser, M. Bloesch, and M. Hutter, “Probabilistic terrain mapping for mobile robots with uncertain localization,” *IEEE Robotics and Automation Letters*, vol. 3, no. 4, pp. 3019–3026, 2018.
- [76] W. Burgard, M. Moors, C. Stachniss, and F. E. Schneider, “Coordinated multi-robot exploration,” *IEEE Transactions on robotics*, vol. 21, no. 3, pp. 376–386, 2005.
- [77] B. Yamauchi, “A frontier-based approach for autonomous exploration,” in *Proceedings 1997 IEEE International Symposium on Computational Intelligence in Robotics and Automation CIRA’97: Towards New Computational Principles for Robotics and Automation*. IEEE, 1997, pp. 146–151.
- [78] F. Allgöwer and A. Zheng, *Nonlinear model predictive control*. Birkhäuser, 2012, vol. 26.
- [79] J. Gregory, J. Fink, E. Stump, J. Twigg, J. Rogers, D. Baran, N. Fung, and S. Young, “Application of multi-robot systems to disaster-relief scenarios with limited communication,” in *Field and Service Robotics*. Springer, 2016, pp. 639–653.
- [80] S. Johnson, “The NLOpt Nonlinear-Optimization Package,” <http://ab-initio.mit.edu/nlopt>.

- [81] M. Likhachev, D. I. Ferguson, G. J. Gordon, A. Stentz, and S. Thrun, "Anytime dynamic a*: An anytime, replanning algorithm." in *ICAPS*, vol. 5, 2005, pp. 262–271.